Cessation of a dense granular flow down an inclined plane

S. Bharathraj and V. Kumaran
Department of Chemical Engineering, Indian Institute of Science, Bangalore 560 012, India

(Received 15 June 2018; published 4 February 2019)

The cessation of a dense granular flow down an inclined plane upon decrease in the angle of inclination is studied using particle-based simulations for the linear and Hertzian particle contact models for ordered and disordered flows. The nature of the flow is examined by progressively decreasing the angle of inclination by fractions of a degree, with the objective of examining the range of angles for which the hard-particle model can be used to describe the flow and the nature of the flow dynamics very close to cessation where the hard-particle approximation fails. For a disordered flow, when the angle inclination exceeds the angle for flow cessation by about 0.5° for the linear contact model and about 1° for the Hertzian model, the flow is well described by Bagnold rheology, and the Bagnold coefficients are independent of layer height and the particle stiffness, implying that the flow dynamics is well described by the hard-particle approximation. When the angle of inclination exceeds the angle for flow cessation by less than 0.5° for the linear contact model and 1° for the Hertzian contact model, the flow transitions into a layered state consisting of a faster shearing zone of height about 30 particle diameters atop a bottom slowly shearing zone. There are sinusoidal oscillations in the velocity of the center of mass of the flow, and the period of these oscillations is proportional to the characteristic time for particle interactions, indicating that the particle contact time does affect the dynamics of the layered flow. The flow evolution is qualitatively different for an ordered flow. In this case, there is an abrupt transition from a Bagnold flow to a plug flow with sliding at the base when the angle of inclination is decreased by 0.05°. There is no discernible intermediate flow regime where the particle contact time becomes relevant. We also examine the deceleration of the flow when the angle of inclination is decreased from a flowing state to a final angle below the cessation angle. The initial decrease in the flow velocity is exponential for both contact models and for all final angles of inclination. This is followed by a more rapid decrease to the static state. The time constant for the initial decrease is significantly higher for an ordered flow in comparison to a disordered flow. The time constant is independent of the contact model and particle stiffness, and increases with height proportional to $h^{3/2}$, as expected for the hard-particle model.

DOI: 10.1103/PhysRevFluids.4.024301

I. INTRODUCTION

A conceptual basis often used for the study of dense granular flows is the "hard-particle" approximation, where the interactions between particles are considered to be instantaneous collisions. Since the time of an interaction is zero in the hard-particle limit, there is no material timescale. The equilibrium configurations of dense hard-particle fluids have been studied for some time now [1–4]. More recently, the nonequilibrium steady states of hard-particle fluids have been used as models for dense granular flows. For a sheared granular medium, the only relevant timescale is the inverse of the strain rate. From dimensional analysis, all components of the stress are proportional to the square of the strain rate. This relationship between the stress and strain rate, called the Bagnold law [5,6], is found to be applicable for granular flows down an inclined plane even when the flow is dense and

the coordination number (number of particles in simultaneous contact with a test particle) is 2 or greater [7–9]. Thus, the constitutive relations are applicable over a wider range of particle volume fraction than that for which the assumption of binary interactions is valid, provided the stiffness of the particle contacts is sufficiently large. The Bagnold relations become inapplicable only when the stiffness of the particle contacts is reduced to very low values, about 10^4–10^5 smaller than those applicable for materials of practical importance such as steel and glass [10].

A. Kinetic theory for granular materials

There has been a lot of theoretical development based on kinetic theory of gases [11] for homogeneously cooling granular materials [12–19], dilute granular materials driven by shear [20–29] or vibration [30–36], and dense granular flows. These have been described using conservation equations for mass, momentum, and energy similar to those for molecular gases. At the microscopic level, the main difference between granular and molecular gases is that the interactions between molecules are energy conserving, whereas kinetic energy is dissipated in an interaction between two grains due to the inelastic nature of the collisions. The energy equation for a granular gas contains an energy dissipation term due to inelastic collisions between particles and therefore a constant supply of energy is necessary to maintain a steady flow. This energy is provided either by forcing from the boundaries, as in the case of a vibrated granular material, or by mean shear, as in the case of the flow down an inclined plane. Constitutive relations for the stress and the heat flux, which incorporate the effect of inelasticity, have been derived up to Burnett order for a granular flow [24,25]. The theory has been extended to dense gases using the Enskog approximation [37–41] for the two-particle distribution function. For dense flows, it has been realized that the molecular chaos approximation in the Boltzmann and Enskog descriptions are not valid, and the effect of correlations have also been included in deriving constitutive relations [42–44].

B. Flow down inclined plane

The granular flow down an inclined plane is a widely studied example of a dense granular flow, because simulations and experiments have revealed that it exhibits many unusual features [45–48]. At steady state, the flow is characterized by a constant ratio of the shear and normal stress, which is proportional to the ratio of the body forces parallel and perpendicular to the base. In simulations, the volume fraction of the particles is a constant independent of depth, in contrast to the expected increase in volume fraction with depth due to the increased overburden. A stable flow is obtained only for a limited range of angles of inclination, and the minimum angle for flow initiation decreases as the height of the layer increases [47]. The velocity profile in the bulk is independent of the base configuration or the conditions at the base and is described by the Bagnold law. However, there are temperature boundary layers at the top and bottom where the Bagnold law does not apply, because the rate of conduction of energy is comparable to the rates of production and dissipation [49].

Constitutive relations obtained from the hard-particle description have been remarkably successful in capturing the salient features of the granular flow down an inclined plane [49,50]. These kinetic models do predict the constant volume fraction with height, the initiation of flow at a finite angle of inclination, the applicability of the Bagnold relation in the bulk, and the effect of the base configuration on the flow dynamics. The coefficients in the Bagnold relations have been quantitatively predicted by incorporating the effect of correlations in the particle velocities in a kinetic theory description [41].

The initiation and cessation of flow for thin layers up to about 40 diameters in height was considered by Silbert *et al.* [51]. The initiation and cessation of flow was found to be qualitatively different for thin (thick) layers with thickness less (more) than about 20 particle diameters. For thick layers, during flow development from a stationary state, there is a shearing layer at the bottom which supports a plug on top. The thickness of the shearing region increases and encompasses the entire layer as flow develops. During cessation of flow, there is deceleration at the bottom first, and

the static zone at the bottom expands upward until flow stops. Here, two related phenomena are analyzed. The cessation of flow is analyzed for thick layers, in order to examine how the rate of decrease of the velocity and the timescale for cessation depends on the system parameters for layers of height greater than the 35 particle diameters. In addition, the steady flow for angles very close to the angle of cessation is considered.

C. Constitutive models

The hard-particle approximation is also the basis of the $\mu(I)$ rheology [52–54], where the friction coefficient μ, the ratio of the shear stress and pressure, is expressed as a function of the inertia parameter I which is $(\dot{\gamma} d/\sqrt{p/\rho})$, where $\dot{\gamma}$ is the strain rate, d is the particle diameter, p is the pressure (or normal stress), and ρ is the density. In this description, the granular material is static when μ is below a minimum value, while there is flow when μ exceeds a certain minimum value. There is usually also a maximum limit for μ for $I \to \infty$, indicating that the ratio of shear and normal stresses cannot exceed a maximum value. The $\mu(I)$ rheology is a generalization, to flowing states, of the critical state theory [55] which provides a yield criterion for static granular materials. The $\mu(I)$ rheology can be derived from Bagnold rheology and is therefore based on the assumption that the only relevant time cale is the inverse of the strain rate. However, the $\mu(I)$ relationship only provides one relation among the shear stress, pressure, and strain rate. Therefore, it is not possible to evaluate the stress and pressure from I. More recently, an empirical relation has also been used to relate the volume fraction ϕ to the inertia number I [56]. This approach is useful if the pressure is specified on the basis of the overburden, for example, but is more difficult to implement in complex flows where there are complicated variations of the pressure with position, because there is only one relation among three quantities, pressure, shear stress, and the inertia parameter. In order to fix the pressure, the constant density condition is usually used, and this results in a pressure Poisson equation [54]. This is applicable only when the volume fraction is nearly a constant for very dense flows and is at variance with the $\phi(I)$ relation, which predicts that the volume fraction varies with I.

It is known that the $\mu(I)$ constitutive relations could exhibit short wavelength instabilities under certain conditions [57]. There have been extensions of the $\mu(I)$ rheology to include a microscopic length scale in the problem [58]. These follow earlier interpretations of a microscopic length scale in the flow, such as the region of rotational disequilibrium between the particle spin and the material deformation [59,60]. A microscopic length scale, the conduction length, does emerge naturally from kinetic theory based constitutive relations, and this has been used to successfully explain the variation in the flow properties near boundaries [10,49,61]. The extensions of the $\mu(I)$ rheology, and other theories which postulate a microscopic length scale, still do not contain a material timescale, and so they are consistent with hard-particle approximation. However, all of these theories contain a material length scale; the square of this length scale multiplies the Laplacian of the dynamical quantity (granular temperature, fluidity, etc.). When the flow length scale is large compared to the material length scale, the diffusion term can be neglected in the bulk of the flow far from boundaries, and the Bagnold relationship is applicable.

Some models have postulated a correlation length between particles that is much larger than the particle size and which could diverge as the system approaches cessation or a critical point [62,63]. While theories based on large or diverging correlation lengths [37,38,62,63] have been able to capture the dynamics of a range of granular flows, attempts to measure a correlation length in simulations have not been as successful [64]. In such cases, the correlation length has to be considered the material scale, and the minimum system size for Bagnold rheology increases as the length scale increases.

D. Jamming and flow cessation

A boundary between a flowing and a static region is often observed in granular flows in hoppers and chutes. The boundary is often not static but is formed by a dynamical balance between erosion

and deposition [65]. In some cases, such as the flow in a rotating drum, the flow occurs in a series of avalanches at low rotation rates. Even in cases where distinction between the steady flow and the static region is clear, there are episodic rearrangements in the static region. Kinetic models based on the hard-particle approximation have been fairly successful in describing the flowing state of dense granular materials, but in these models, flow cessation occurs at a fixed ratio of the shear and normal stresses. The coexistence of the flowing and static states, and the conditions at the interface between the flowing and static states, is one of the important inputs required for formulating continuum equations and boundary conditions for flowing granular materials. An important issue is whether the flow can be described by the hard-particle approximation down to the static region, or whether there is an intermediate region where it is necessary to account for the finite stiffness of the particles.

Hard-particle systems comprise a singular limit where the force between particles is infinite when there is overlap and zero when there is no overlap. It is known that the random close packing volume fraction, 0.64, is the maximum attainable volume fraction for a random assembly of hard spheres, though an equilibrium system undergoes a crystallization transition at a volume fraction of 0.49. Different aspects of the random close-packed state have been studied, such as the Voronoi volume distributions and the configurational entropy [4], but there is still uncertainty regarding the nature of the transition, and whether the random close packed state is a unique state [66]. A random close-packed system is in an isostatic state, where the number of degrees of freedom is equal to the constraints. This requires that the coordination number (number of particles in simultaneous contact with a test particle) is 4, on average, for frictional particles in three dimensions. When the volume fraction is decreased from the random close-packed state, a hard-particle system is in the instantaneous collision regime, since the period of interaction is zero for an ideal hard-particle system. Therefore, the coordination number undergoes a discontinuous increase from 0 to 4 at the transition from the flowing to the static state for hard-particle systems.

Due to the discontinuous transition from an isostatic state to Bagnold rheology in hard-particle models, the boundary between flowing and static regions is necessarily a surface of infinitesimal thickness separating static regions from those where particles interact through instantaneous collisions. In real systems, it is possible that as the ratio of shear and normal stress decreases, the system transitions to a regime of non-Bagnold rheology where the material timescale, based on the particle stiffness, is a relevant parameter. The range of stress ratios for non-Bagnold rheology is likely to determine the thickness of regions where there is a transition from static to flowing states.

In order to obtain insight into the transition between flowing and static states, we examine here the cessation of a dense granular flow down an inclined plane as the angle of inclination is decreased. The cessation of flow is a fascinating phenomenon superficially similar to the jamming in dense suspensions or granular materials [67,68]. While the maximum random close-packing volume fraction for spherical particles is about 0.64, the jamming phenomenon is observed in sheared suspensions at a lower volume fraction of about 0.59. In the jamming transition, the stress of a sheared suspension diverges with an increase in the strain rate, and this divergence occurs when the strain rate exceeds a critical value. The divergence in the stress is considered to be the consequence of the formation of "force chains" due to frictional contact between particles, and interparticle frictional is considered essential for jamming [69,70]. The cessation of a granular flow over an inclined plane is qualitatively different, because there is a free surface. The particle forces necessarily decrease to zero at the free surface; it is not possible to have sample-spanning force chains in this case. Yet, there is the cessation of flow, and the maximum volume fraction in the flowing state is found to be about 0.59. This observation of an increase in the volume fraction at flow cessation is also incorporated in critical state theories for soil mechanics [55], where the material which is densely packed expands upon the application of shear.

E. Order-disorder transition

Recent research has revealed [61,71–73] that there are two distinct types of flows down an inclined plane, the ordered flow and the disordered flow. The effect of base roughness on the flow

rule for thin layers [74] and the order-disorder was considered in the earlier studies [61], where the base roughness was defined as the ratio of the base and moving particle diameter for frozen-particle bases and the amplitude of the base oscillation for sinusoidal bases. It was shown that there is a discontinuous transition from a disordered to an ordered flow when the base roughness is decreased by less than 1% for different base topographies. The properties of ordered and disordered flows are very different. An ordered flow consists of layers of particles parallel to the base sliding over each other, and there is hexagonal packing within the layers. In the disordered flow, the relative configuration of the particles is random. The velocity profile is a Bagnold profile for both ordered and disordered flows, but the Bagnold coefficients for the ordered flow are two orders of magnitude lower than those for the disordered flow. In the bulk of the flow, the ratio of the granular temperature and the square of the strain rate is a constant, as expected for a hard-particle system. It is now known that the transition between ordered and disordered flows is a hard-particle phenomenon. When the particle stiffness is decreased below the threshold value for Bagnold rheology, it has been observed in simulations that there is no order-disorder transition [10]. A continuum model for a layered fluid has been used to predict the scaling of the transition base roughness on the wavelength of the base modulation for sinusoidal bases [61].

F. Present study

The dynamics of the inclined plane flow is examined as the angle of inclination is decreased close to the angle for flow cessation. The simulations are carried out for two contact models, the linear (Hookean) and the Hertzian contact model, in order to verify that the phenomena observed are independent of the contact model. The flow height is varied from a minimum of about 35 particle diameters to a maximum of about 140 particle diameters. The particle stiffness is varied over two orders of magnitude, in order to examine whether the contact time influences the flow dynamics. The minimum value of the scaled particle stiffness used here, 10^6 for the linear and Hertzian contact model, is sufficiently large that the system is in the hard-particle regime for the flowing state even when the angle of inclination is 1° above the angle for flow cessation [10].

In the first series of simulations, the angle of inclination is decreased in intervals of a fraction of a degree close to flow cessation, for both ordered and disordered flows. Simulations are necessary for this study, since it is infeasible to carry out such a gradual decrease in the angle of inclination in repeatable experiments. These simulations enable us to determine whether there are intermediate regimes between the Bagnold flow and the static state and to examine the dynamics of these flows.

A limitation of these simulations is that it is not possible to capture phenomena such as avalanches due to the small system size. An avalanche is a large mass that slides down a slope. In a periodic cell, the mass that leaves the cell on the downstream side enters on the upstream side, so it is not possible to simulate a large mass that slides downward. Only spatially invariant flows can be simulated in a periodic cell, and therefore our simulations are restricted to spatially invariant steady or time-varying flows. Another limitation is that the simulations do not capture hysteretic effects, that is, the difference in the angle of inclination between flow initiation (as the angle of inclination is increased) and the flow cessation (when the angle of inclination is decreased). Hysteresis is a complicated phenomenon not completely understood, and possible explanations are the cohesive forces between particles in the static state or the difference between the static and dynamic friction coefficient. Here, the focus is on flowing states close to cessation, and so we consider the possibility of cohesion or the difference between static and dynamic angles of friction. Here, we find the same flowing states whether the angle of inclination of an initially static state is increased or whether the angle of inclination of a flowing state is decreased. This is provided that the flow development time is sufficiently large; the details of the development and averaging time are provided in Sec. III.

A second series of simulations involves the cessation of flow from an initial steady state at an angle of 22° to lower angles of inclination, both for a final static state and for a final flowing state. The deceleration of the flow is examined in order to determine whether, and to what extent, the hard-particle model can be used to describe the flow cessation.

II. SIMULATION METHODOLOGY

The simulations are carried out using the LAMMPS molecular dynamics simulation software using the Hookean (linear) and the Hertzian spring-dashpot-slider model [75] for the particle-particle and particle-wall interactions. Spherical particles of mass m and diameter d are used in the simulations. For flows driven by gravity, it is convenient to nondimensionalize the mass dimension by the particle mass m, length by the particle diameter d, time by $\sqrt{d/g}$, and velocity by $\sqrt{gd}$, where g is the acceleration due to gravity. In the following analysis, all quantities are expressed in dimensionless form.

The force between the particles is zero when the distance between the particle centers is greater than the particle diameter. When the distance between particles is less than the particle diameter, the overlap between particles δ_n is defined as the difference between the particle diameter and the distance between the centers. The normal contact force, which acts along the line joining the centers of the particles, consists of a spring force which depends on the overlap and a damping force which depends on the relative velocity of the particles. For the linear contact model, the spring force is proportional to the overlap δ_n, while the damping force is proportional to the relative normal velocity. For the Hertzian contact model, the spring force is proportional to $\delta_n^{3/2}$, and the damping force is proportional to $\delta_n^{1/2}$ times the normal velocity. The resistive force tangential to the surfaces of contact depends on the tangential displacement $\mathbf{u}_t$, the vector displacement of the point of contact in the direction tangential to the surfaces since the initiation of contact, and the tangential relative velocity. For the linear model, the tangential spring force is proportional to $\mathbf{u}_t$, and the damping force is proportional to the tangential relative velocity. For the Hertzian model, the tangential spring force is proportional to $\delta_n^{1/2}\mathbf{u}_t$, and the damping force is proportional to $\delta_n^{1/2}$ times the relative tangential velocity. For calculating the tangential force, the contacts are separated into two types, sticking and sliding contacts. If the ratio of tangential and normal force magnitudes, using the spring-dashpot model, is greater than the friction coefficient μ, the contact is considered to be a sliding contact, and the tangential force is set equal to μ times the normal force. If the ratio of the tangential and normal force magnitudes is less than μ, the contact is considered to be a sticking contact, and the tangential force computed from the spring-dashpot model is used. The details of the expressions of the contact forces have been provided earlier [7,45,72], and so they are not repeated here.

There are five constants in the models for the particle interactions, the spring constants k_n and k_t in the normal and tangential directions, the damping constants γ_n and γ_t, and the friction coefficient μ. It was shown earlier [10] that the flow is in the hard-particle regime when the scaled restitution coefficient k_n is 10^6 or higher for the linear and Hertzian models. Since we are interested in the cessation of flow for hard-particle systems, two values of the scaled restitution coefficient k_n, 10^6 and 10^8, are used for the linear and Hertzian models. The ratio (k_t/k_n) is set equal to $(2/7)$ in all the simulations. The value of γ_n, the normal damping coefficient, is chosen so that the normal coefficient of restitution (ratio of post- and precollisional velocities along the line joining centers) for an interaction between a pair of particles is 0.6 for the linear contact model. The same numerical value is used for γ_n for the Hertzian contact model as well. The ratio of the damping coefficients in the tangential and normal directions, (γ_t/γ_n), is set equal to $(1/2)$. The friction coefficient is set equal to 0.4. The reasons for the specific choice of parameters has been discussed extensively earlier [10,45,61].

The time period of an interaction, τ_c, is an important parameter that is used later in the analysis. For the linear contact model, the contact time τ_c for a binary contact between two particles is independent of the precollisional velocity, and is equal to $\pi(2k_n/m - \gamma_n^2/4)^{-1/2}$. The normal coefficient of restitution e_n, which is the ratio post- and precollisional relative velocities along the line joining the centers of the particles, is independent of the precollisional velocity, and is equal to $\exp(-\gamma_n\tau_c/2)$ for the linear contact model. The contact time for the Hertzian contact model does depend on the precollisional velocity. For the present purposes, an average contact time is defined based on the average overlap $\bar{\delta_n}$ between particles for the Hertzian contact model. The average contact time is defined as $\pi(2k_n/m - \gamma_n^2/4)^{-1/2}\bar{\delta_n}^{-1/4}$ [10], where $\bar{\delta_n}$ is the average overlap between the particles. The values of $\bar{\delta_n}$ are determined as described in Ref. [10].

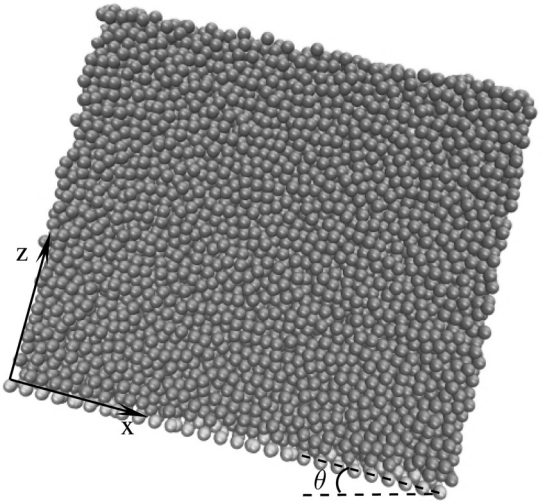

FIG. 1. The configuration and coordinate system used for the analysis.

III. SYSTEM CONFIGURATION

The system consists of the steady flow of a granular material down an inclined plane, where x is the flow direction, z is perpendicular to the base, and y is perpendicular to the flow and parallel to the base, as shown in Fig. 1. Periodic boundary conditions are used in the x and y directions, while there is fixed base at the bottom and a free surface on top in the z direction. In most of the simulations, the simulation box dimension is 40 particle diameters in the x direction and 20 particle diameters in the y direction. However, simulations have been carried out with box sizes up to 80 particle diameters in the x direction and 40 particle diameters in the y direction, in order to examine system size effects. Different system sizes, consisting of 32 000, 48 000, 64 000, 96 000, and 128 000 particles with heights approximately 35, 48, 70, 100, and 140 particle diameters, respectively, have been simulated.

The effect of base topography on the order-disorder transition has been studied earlier [61] for different base topographies, including random and hexagonally ordered frozen-particle bases and sinusoidal bases. That study revealed that the order-disorder transition takes place as the base roughness is increased for all base topographies, and the flow in the bulk is independent of base topography. However, there is a large increase in the granular temperature in a temperature boundary layer near the base for sinusoidal bases, and there is substantial slip at the base. In the case of frozen-particle bases, the temperature is comparable to that in the bulk. The objective of the present study is to examine the flow behavior in the bulk as the angle of inclination is decreased. In order to avoid a large temperature gradient at the base, the configuration is restricted to frozen-particle bases. In most of the simulations, hexagonally ordered frozen particles of diameter 0.5 and 1.5 are used as the base configuration to generate ordered and disordered flows respectively.

Two different types of simulations are carried out. Initially, the base is horizontal, and the particles are dropped into the box by sequential deposition in a random configuration. This is then used as the initial condition. For the flow near cessation, the box is tilted to the desired angle of inclination, and the flow progresses until steady state is attained. The simulation progresses in times steps of $(\tau_c/50)$ for both the linear and Hertzian models. The flow development time is typically $2.25 \times 10^3\sqrt{d/g}$, which is sufficient for the flow to reach steady state close to cessation. Averages are calculated over an additional time period of $4 \times 10^2\sqrt{d/g}$. Since the angles of inclination are close to the angle of cessation, care is taken to ensure that the flow development time is sufficiently long. For comparison, for real particles of diameter 1 mm, the development time used here is about

200 s, and averages are calculated over an additional period of about 40 s. For the simulations on the cessation of flow, the simulation cell is first tilted at an angle of 22°, and the simulation is run until steady state is reached. After this, the angle is instantaneously decreased to a lower value, and the evolution of the velocity and other dynamical quantities is recorded as a function of time.

The quantities reported here are the mean velocity v_x, the granular temperature T, and the coordination number Z as a function of the height z. The averages are calculated over height intervals of 4 particle diameters in the z direction. The coordination number is the average number of particles in simultaneous contact with a test particle, while the mean velocity, angular velocity, and granular temperature are defined as

$$\boldsymbol{v} = \frac{1}{N}\sum_{i=1}^{N} \boldsymbol{v}^{(i)}, \quad \boldsymbol{\omega} = \frac{1}{N}\sum_{i=1}^{N} \boldsymbol{\omega}^{(i)}, \quad T = \frac{1}{6N}\sum_{i=1}^{N} (\boldsymbol{v}^{(i)} - \boldsymbol{v})^2 + I(\boldsymbol{\omega}^{(i)} - \boldsymbol{\omega})^2. \tag{1}$$

Here, N is the total number of particles in the volume of height 4 particle diameters in the z direction, and the extent of the simulation cell in the x and y directions, $\boldsymbol{v}^{(i)}$ and $\boldsymbol{\omega}^{(i)}$ are the velocity and angular velocity of particle i, and I is the moment of inertia which is $(1/10)$ when scaled by suitable powers of the particle mass and diameter for uniform spheres. Some time-dependent average quantities are also defined for the analysis of the flow deceleration due to a decrease in the angle of inclination. The velocity of the center of mass for the entire layer is defined as

$$\mathbf{v}^{\text{c.m.}}(t) = \frac{1}{N_p}\sum_{i=1}^{N_p} \mathbf{v}_i, \tag{2}$$

where N_p is the total number of particles and $\mathbf{v}_i$ is the velocity of particle i. The time average of the velocity of the center of mass (c.m.) is

$$\bar{\mathbf{v}}^{\text{c.m.}} = \frac{1}{T_{\text{av}}}\int_0^{T_{\text{av}}} dt\ \mathbf{v}^{\text{c.m.}}(t), \tag{3}$$

where T_{av}, the averaging time, is much longer than the time for fluctuations. The fluctuating velocity of the center of mass is defined as

$$\mathbf{v}^{\text{c.m.}'} = \mathbf{v}^{\text{c.m.}} - \bar{\mathbf{v}}^{\text{c.m.}}. \tag{4}$$

The mean square of the fluctuating velocity and the fluctuating energy are defined as

$$\overline{\mathbf{v}^{\text{c.m.}'2}} = \frac{1}{T_{\text{av}}}\int_0^{T_{\text{av}}} dt\ (\mathbf{v}^{\text{c.m.}'}(t))^2. \tag{5}$$

IV. KINETIC MODELS FOR HARD-PARTICLE SYSTEMS

For the steady flow down an inclined plane with no variations in the streamwise (x) and spanwise (y) directions, the momentum conservation equations in the x and z directions are

$$\frac{d\sigma_{xz}}{dz} + \rho g_x = 0, \quad \frac{d\sigma_{zz}}{dz} + \rho g_z = 0, \tag{6}$$

where σ_{xz} and σ_{zz} are the components of the stress tensor, ρ is the density, and g_x and g_z are the components of the gravitational acceleration in the x and z directions. Note that g_z is negative for the coordinate system shown in Fig. 1. The Bagnold relations for the stress tensor are

$$\sigma_{xz} = B_{xz}\left(\frac{dv_x}{dz}\right)^2, \quad \sigma_{zz} = -B_{zz}\left(\frac{dv_x}{dz}\right)^2, \tag{7}$$

where B_{xz} and B_{zz} are the Bagnold coefficients. The Bagnold coefficients depend on the volume fraction but not on the flow velocity or the strain rate. The Bagnold velocity profile is obtained by

solving Eq. (6) using the constitutive relation (7),

$$v_x = v_s + \frac{2}{3}\sqrt{\frac{\rho g_x h^3}{B_{xz}}}\{1 - [1 - (z/h)]^{3/2}\}, \tag{8}$$

where h is the total height of the flowing layer and v_s is the slip velocity (if any) at the base.

In the hard-particle model for a sheared granular flow, the granular temperature T [Eq. (1)] is proportional to the square of the strain rate [61] in the bulk when there is a balance between the production of fluctuating energy due to mean shear and the energy dissipation due to inelastic collisions. Based on the kinetic theory of gases, the normal and shear stresses can be expressed as

$$\sigma_{xz} = \frac{\mu_\phi T^{1/2}}{d^2}\frac{dv_x}{dz}, \quad \sigma_{zz} = -\frac{p_\phi T}{d^3}, \tag{9}$$

where μ_ϕ and p_ϕ are dimensionless functions of the volume fraction and the interparticle coefficient of restitution. The rate of dissipation of energy per unit volume is given by

$$D = \frac{D_\phi T^{3/2}}{d^4}, \tag{10}$$

where D_ϕ is a dimensionless function of the volume fraction and interparticle interaction parameters. In the bulk of the flow far from boundaries, there is a balance between the rate of production of energy due to the mean shear, $\sigma_{xz}(dv_x/dz)$, and the rate of dissipation of energy [49]. Because of this balance, the granular temperature is proportional to the square of the strain rate,

$$T = (\mu_\phi d^2/D_\phi)(dv_x/dz)^2. \tag{11}$$

This proportionality between the granular temperature and the strain rate during the cessation of flow is examined in Sec. VI.

V. FLOW NEAR CESSATION

A. Mean velocity and granular temperature

The evolution of the velocity profile with angle of inclination close to flow cessation is shown in Fig. 2(a) for a flowing layer with height about 70 particle diameters in a narrow range for the angle of inclination between 19.5° and 19.9°. The corresponding granular temperature profiles are shown in Fig. 2(b), and the coordination number profiles are shown in Fig. 2(c). Two distinct flow regimes are visible in Fig. 2. There is no flow when the angle of inclination is 19.5° or lower, and the granular temperature is zero. When the angle of inclination is 19.8° or higher, there is shearing throughout the bulk, and the velocity profile is well approximated by the Bagnold profile [Eq. (8)], as shown in Fig. 2(a). The granular temperature increases linearly with depth, as expected for a Bagnold flow. This regime is referred to as the "Bagnold flow" regime. When the angle of inclination is in the range 19.55° to 19.75°, there is a higher strain rate within a layer of height about 30 particle diameters at the top, and the velocity profile is a combination of two distinct profiles, one with a higher slope and an upward curvature at the top and a second with a lower slope at the bottom. The granular temperature is near constant in the flowing layer of thickness about 30 particle diameters at the surface, but it decreases to a lower value in the region with lower shear rate at the bottom. This regime with a velocity profile that is concave upward in the $u_x - z$ graph, which precedes flow cessation as the angle of inclination is decreased, is called the "layered flow" regime. The distinct Bagnold flow and layered flow regimes are also observed for the Hertzian contact model, as shown in Fig. 3. In this case, there is no flow when the angle of inclination is 18.9° or lower. The layered flow regime is observed for a larger range of inclination angles, from about 19° to about 20°, and there is a transition to the Bagnold flow regime when the angle of inclination is 20.1° or above. The velocity profile is well fit by the Bagnold profile, and the temperature decreases linearly with height in the Bagnold flow regime. The qualitative features of the flow in the layered flow regime, with two

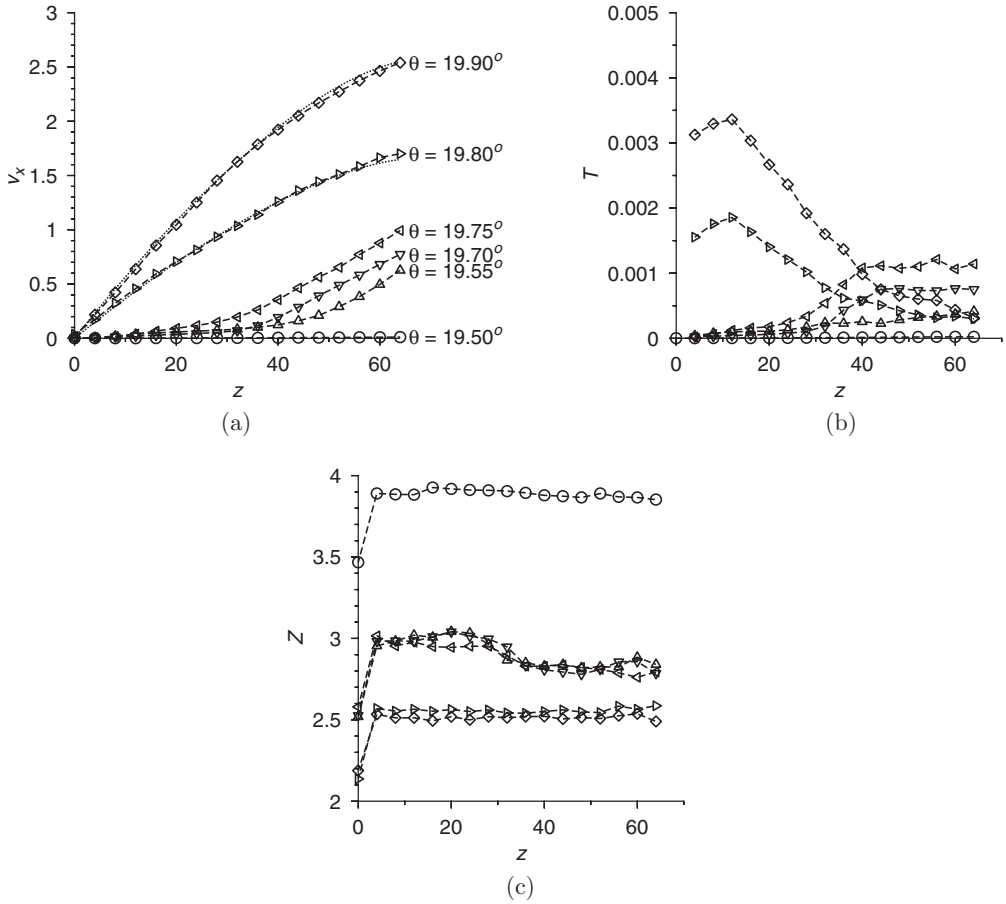

FIG. 2. The mean velocity (a), granular temperature (b), and the coordination number (c) for the flow down an inclined plane at angles of inclination 19.50° (○), 19.55° (△), 19.70° (▽), 19.75° (◁), 19.80° (▷), and 19.90° (◇). The dotted lines in panel (a) show fits to Bagnold profiles for the two highest angles.

distinct velocity and temperature profiles in the upper and lower regions, are qualitatively similar to those for the linear contact model.

The profiles of the coordination number also show very different characteristics in the Bagnold flow and the layered flow regimes. When there is no flow at angle 19.5° or lower for the linear contact model and 18.9° or lower for the Hertzian contact model, the coordination number is close to 4 throughout the height of the layer. The coordination number is significantly smaller within a layer of particles near the base, because the particle contacts with the frozen base particles are not included in the computation. It should be noted that the preparation of a static configuration by pouring from the above results in vibrations at the contacts which take a long time to dampen due to energy dissipation at the contacts. For particles with high stiffness, this results in instantaneous breakage and formation of contacts, and the coordination number is significantly smaller than the isostatic value of 4 when vibrations are present. To rapidly damp out vibrations and reach the final static state, a drag force that is linear in velocity has been exerted on the particles. At the inception of flow, the vibrations at contact are re-energized by the particle motion above, and the coordination number decreases to a value significantly smaller than 4 for the isostatic state. Because of this, a sharp decrease in the coordination number is observed when the system transitions from a static to a flowing state, that is, when the angle of inclination is increased from 19.5° to 19.55° for the linear

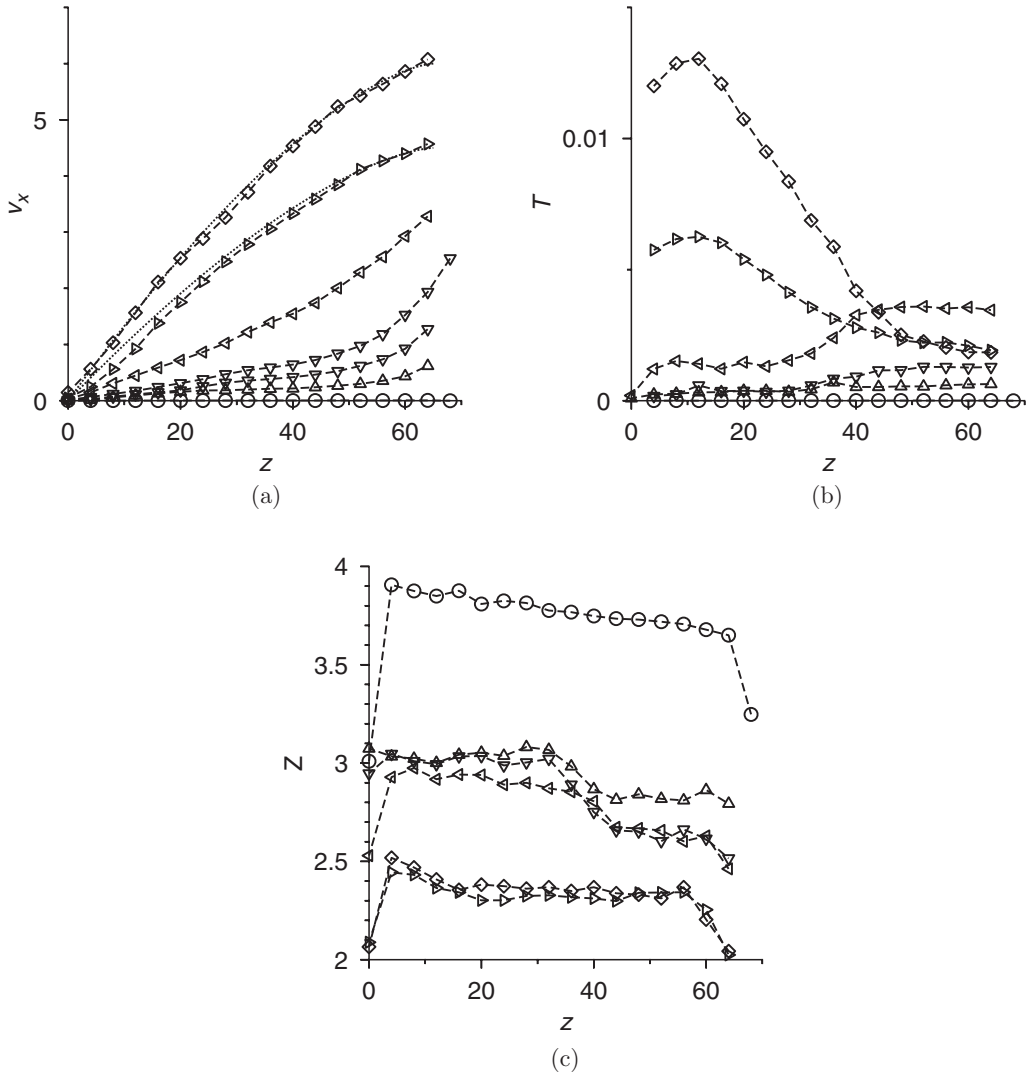

FIG. 3. The mean velocity (a), granular temperature (b), and the coordination number (c) for the flow down an inclined plane at angle of inclination 18.90° (○), 19.00° (△), 19.50° (▽), 20.00° (◁), 20.10° (▷), and 20.20° (◇). The dotted lines in panel (a) show fits to Bagnold profiles for the two highest angles.

model and 18.9° to 19° for the Hertzian model. In the layered flow regime between angles 19.55° and 19.75°, the coordination number has a distinctly lower value in the layer of thickness about 30 particle diameters at the top in comparison to the layer with the lower shear rate at the bottom. Thus, the layering in the strain rate and the granular temperature is also correlated with a layering in the average coordination number. There is a distinct decrease in the coordination number coinciding with the transition from the layered flow to the Bagnold flow regime. In the Bagnold flow regime, the coordination number is observed to be approximately independent of height.

The distinct layered flow and Bagnold flow regimes for the mean velocity and the granular temperature are also observed for flows with other heights that have been studied, from about 35 particle diameters to about 140 particle diameters, as shown in Figs. 4(a)–4(d). The range of angles for the layered and Bagnold flow regimes is a little different for a height of 35 particle diameters—a layered flow is observed for angle in the range 19.5–20.1°, while the Bagnold flow is observed when

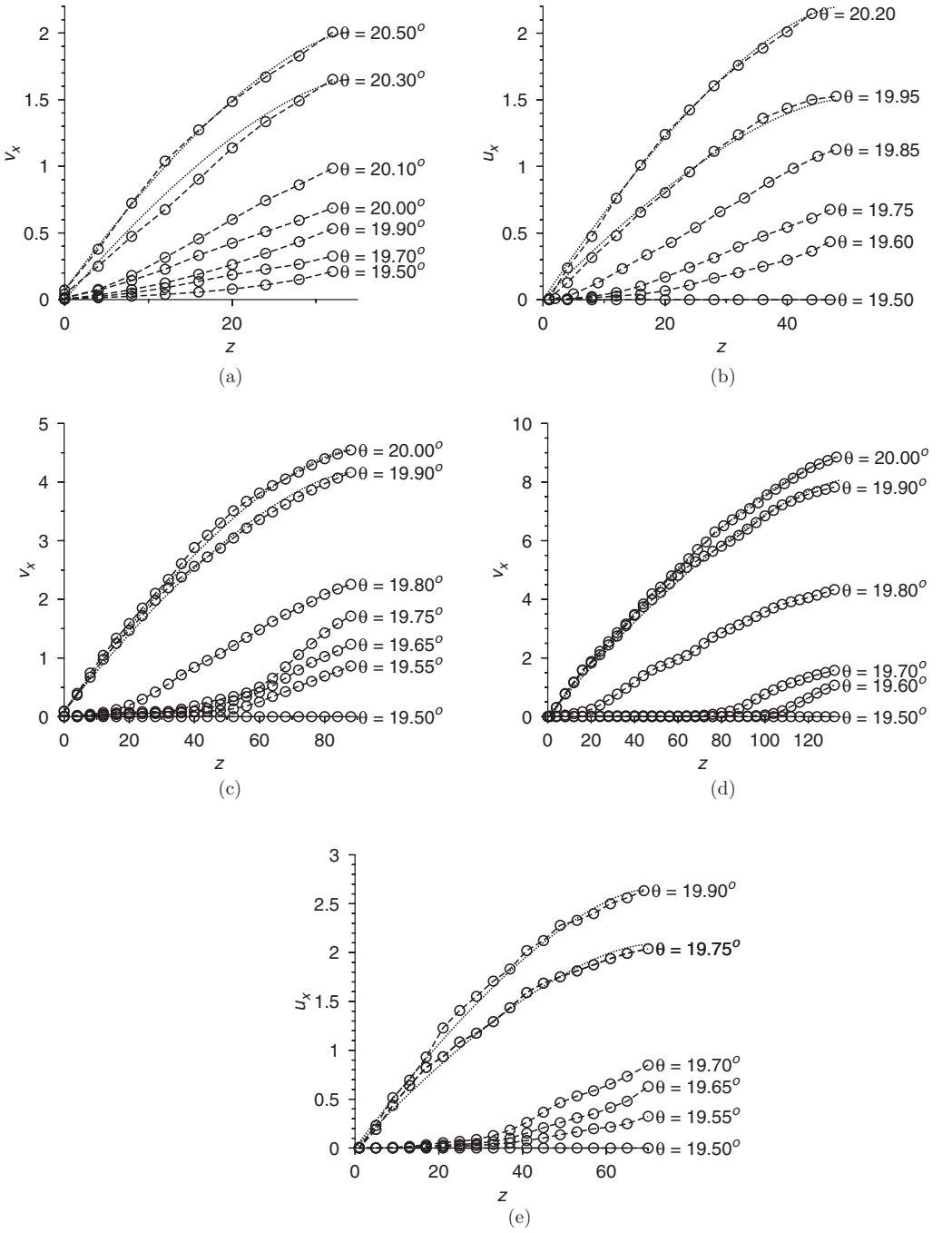

FIG. 4. The mean velocity for different angles of inclination for a flowing layer with height about 35 particle diameters (a), 48 particle diameters (b), 92 particle diameters (c), and 140 particle diameters (d) for the linear contact model with scaled particle stiffness $k_n = 10^6$, and for a flowing layer with height about 70 particle diameters for the linear contact model with scaled spring stiffness $k_n = 10^8$ (e). The dotted lines show the Bagnold fits for the two largest angles of inclination.

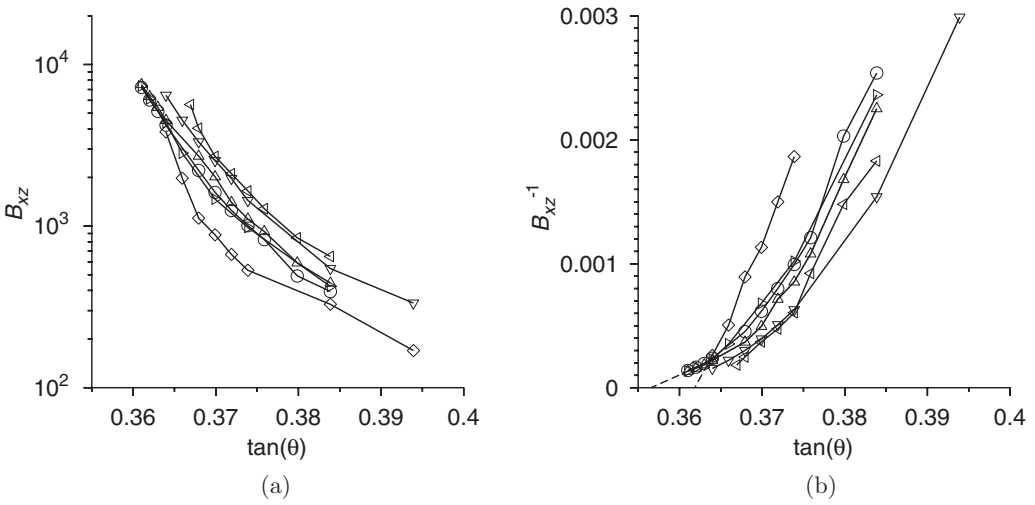

FIG. 5. The variation of the Bagnold coefficient B_{xz} (a) and the inverse of the Bagnold coefficient B_{xz}^{-1} (b) with the tangent of the angle of inclination for the linear contact model with scaled particle stiffness 10^6 and layer height about 100 particle diameters (○), 70 particle diameters (△), 48 particle diameters (▽), and 35 particle diameters (◁), and for the Hertzian contact model with scaled particle stiffness and layer height about 75 particle diameters (◇).

the angle of inclination is above 20.2°. For depth of about 48 particle diameters and higher, the range of angles for layered and Bagnold flows are approximately independent of height. The mean velocity profile for a layer of height about 70 particle diameters with particle stiffness $k_n = 10^8$ is shown in Fig. 4(d). A comparison with the results for $k_n = 10^6$ in Fig. 2(a) indicates that particle stiffness has little effect on the qualitative nature of the average velocity profiles. There are some quantitative differences. The Bagnold profile is observed for $\theta = 19.75°$ and above in contrast to the situation for $k_n = 10^8$, where it is observed for $\theta = 19.8°$ and above. In addition, the jump in the velocity at the transition from layerd to Bagnold flow is greater for $k_n = 10^8$ in comparison to $k_n = 10^6$. However, the qualitative behavior is the same. The transitions in the temperature and coordination number profiles for other depths are qualitatively similar to those shown in Figs. 2 and 3; the details are not provided here for conciseness.

The Bagnold coefficients for the Bagnold flow have been calculated from Eq. (8) using fits shown by the dotted lines in Figs. 2, 3, and 4. The Bagnold coefficient B_{xz} is shown as a function of the $\tan(\theta)$ for different layer heights in Fig. 5(a). Since the ratio of the Bagnold coefficients is the tangent of the angle of inclination, which varies only by about 4% over the range of angles considered in Fig. 5(a), the divergence of the Bagnold coefficient B_{zz} is similar to that for B_{xz}. The Bagnold coefficients for the linear and Hertzian models are very different, indicating that the contact model does affect the Bagnold coefficient, even though the Bagnold law is satisfied for both contact models. For the linear contact model, there is little variation in the Bagnold coefficient with height when the layer height is greater than about 48 particle diameters, but there is some variation in the Bagnold coefficient when the layer height is decreased to about 35 particle diameters. Figure 5(b) shows the inverse of the Bagnold coefficient as a function of $\tan(\theta)$. An extrapolation of the data suggests that $B_{xz} \to \infty$ at $\tan(\theta) = 0.358$, or $\theta = 19.69°$ for the linear model. However, prior to the cessation of flow, there is a transition to a layered flow at $\theta = 19.75°$, as shown in Fig. 2(a). Similarly, for the Hertzian model, an extrapolation of the data suggests flow cessation, $B_{xz} \to \infty$, at $\tan(\theta) = 0.362$, or $\theta = 19.9°$. Before cessation, there is a transition to a layered flow at $\theta = 20°$. Thus, from Fig. 5(b), B_{xz}^{-1} appears to decrease continuously to zero as the angle of inclination is decreased, but there is a small range of angles of about 0.05–0.1° where the system transitions to the layered flow regime before flow cessation.

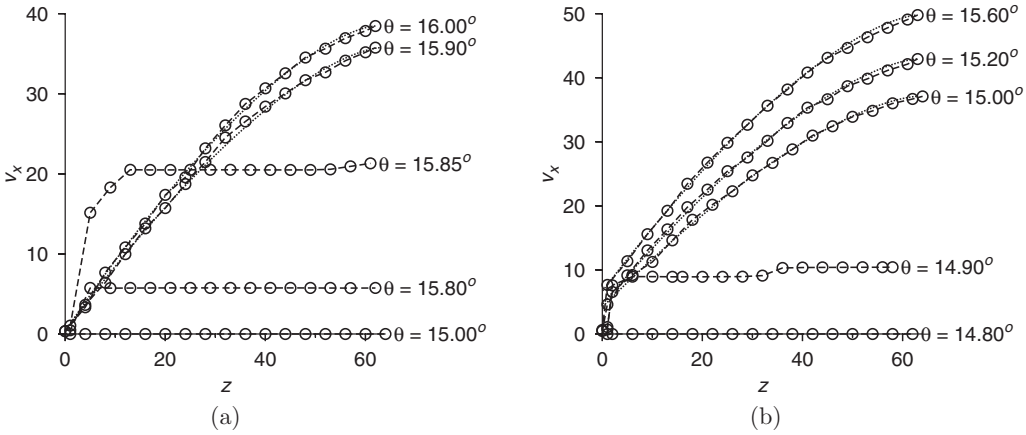

FIG. 6. The mean velocity as a function of height for different angles of inclination for the ordered flow of a layer of height about 65 particle diameters for the linear model (a) and the Hertzian model (b), both with scaled particle stiffness $k_n = 10^6$.

Distinct regimes are not observed for an ordered flow near cessation, as shown in Fig. 6. For the linear model, it is observed that there is no flow when the angle of inclination is 15° or below. When the angle of inclination is between 15° and 15.8°, there is a shearing layer at the bottom and a plug flow on top. The velocity of the plug region exhibits a sharp discontinuous increase when the angle of inclination increases to 15.85°, and there is a discontinuous transition to a Bagnold profile when the angle of inclination is increased to 15.90°. A Bagnold flow is observed for $\theta \geqslant 15.9°$. The range of angles for the plug flow does depend on base roughness for an ordered flow—for a smooth base, there is the flow with shearing at the base and a plug above when the angle is 13°. The angle for inception of flow increases and the slip at the base decreases as the base roughness is increased. However, the angle for transition from the plug flow to the Bagnold flow is independent of the base roughness.

The Bagnold coefficient B_{xz}, calculated using Eq. (8), is shown as a function of the tangent of the angle of the inclination for the ordered flow in Fig. 7(a), and the inverse of the Bagnold coefficient is shown in Fig. 7(b). The inverse of the Bagnold coefficient for the ordered flow appears to start from a finite value at the onset of the Bagnold flow. This is sharp contrast to the disordered flow in Fig. 5, where the inverse of the Bagnold coefficient is numerically small at the onset of the Bagnold regime, and the transition to the stationary state is interrupted by the layered flow. In this sense, the cessation of a disordered flow is much closer to a continuous transition which is cut off by the transition to a layered flow, whereas the cessation of an ordered flow is clearly a discontinuous transition from finite straining to zero straining in the bulk. Since the flow regimes for an ordered flow are limited to the Bagnold and plug flow, we do not analyze these regimes further. The layered flow regime near cessation for the disordered flow is now analyzed in further detail.

B. Contact force distributions

The contact force distributions have to be analyzed with care, because the average contact force increases with depth from the free surface due to the greater overburden. Here the average contact force f_{av} is calculated as the average of the contact force magnitudes for intervals of height 4 particle diameters in the z direction. This average force is then used for scaling the contact forces within the height interval. The probability distribution of the contact force magnitude, $P(f/f_{\text{av}})$, is determined as a function of the ratio (f/f_{av}).

The force distribution is shown as a function of height for a static layer with angle of inclination 19.5° in Fig. 8(a), for a layered flow with angle of inclination 19.6° in Fig. 8(b), and for a Bagnold

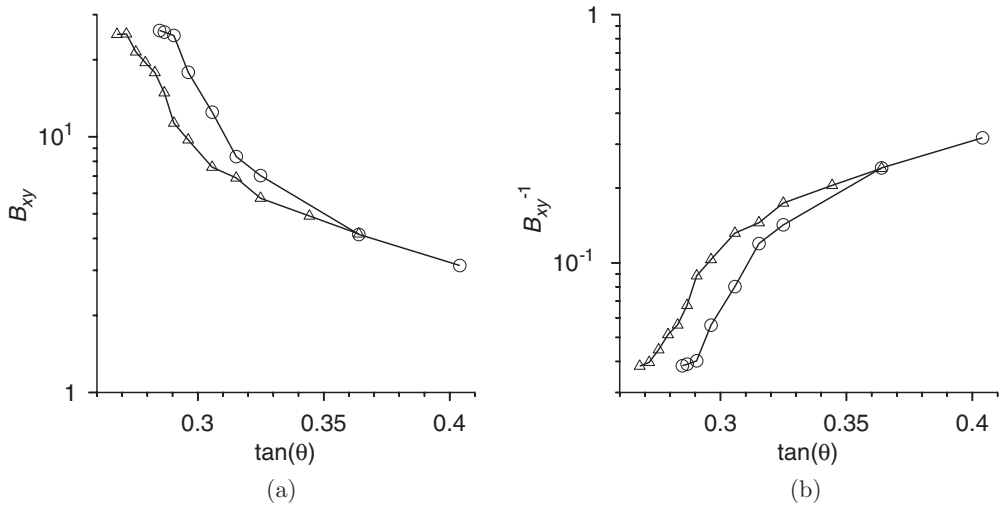

FIG. 7. The Bagnold coefficient (a) and the inverse of the Bagnold coefficient (b) as a function of the tangent of the angle of inclination for the linear contact model (○) and the Hertzian contact model (△), both with scaled particle stiffness $k_n = 10^6$.

flow with angle of inclination 19.9° in Fig. 8(c). For a static layer, the force distribution is close to an exponential distribution with a sharp maximum near zero force, as shown in Fig. 8(a). The force distribution for the Bagnold flow in Fig. 8(c) is also independent of height but is qualitatively different from that for the static state, even though the difference in the angle of inclination is less than 0.5°. The force distribution for the Bagnold flow exhibits a maximum at about $(f/f_{\rm av}) \sim 0.5$, and it exhibits a slower decrease for high force magnitude. For the layered flow, the force distribution in Fig. 8(b) has a distinctly different shape in the region at the bottom (shown by the red lines) and the flowing layer at the top (shown by the blue lines). In the flowing region at $z = 46$ and 62, the force distribution is similar to the distribution for the Bagnold flow in Fig. 8(c), with a maximum at about $(f/f_{\rm av}) \sim 0.5$. At height between $z = 6$ and 26, the shape of the distribution function is different from that for the flowing region above and is similar to that for the static layer in Fig. 8(a).

The force distributions for the Hertzian contact model, for both the static layer [Fig. 9(a)] and the Bagnold flow [Fig. 9(c)] are distinctly different from the corresponding force distributions for the linear contact model, shown in Figs. 8(a) and 8(c). The static force distribution for the Hertzian contact model does show a sharp increase at zero force, but this is less pronounced than that for the linear contact model. The force distribution for the Bagnold flow has a maximum at zero force, as shown in Fig. 9(c), in contrast to the maximum at $(f/f_{\rm av}) \sim 0.5$ for the linear contact model in Fig. 8(c). However, analogous to the situation for the linear contact model, the force distribution for the layered flow in Fig. 9(b) also shows two distinct forms, one corresponding to the static layer at the bottom at $z = 6$ and $z = 26$ (shown by the red lines) and a second corresponding to the flowing layer at the top at $z = 46$ and $z = 62$ (shown by the blue lines). The former is qualitatively similar to the force distribution for the static layer in Fig. 9(a), while the latter bears a resemblance to that for the Bagnold flow in Fig. 9(c). Thus, the distinction between the static and flowing regions in a layered flow is also reflected in the force distributions for the linear and the Hertzian models.

C. Periodic oscillations in the layered flow

In the layered flow regime, superposed on the steady velocity and temperature profiles are unusual time-periodic oscillations, which have not been reported earlier for these types of flows. The variation in the average center-of-mass velocity $\bar{v}_x^{\rm c.m.}$, Eq. (3), with the angle of inclination near

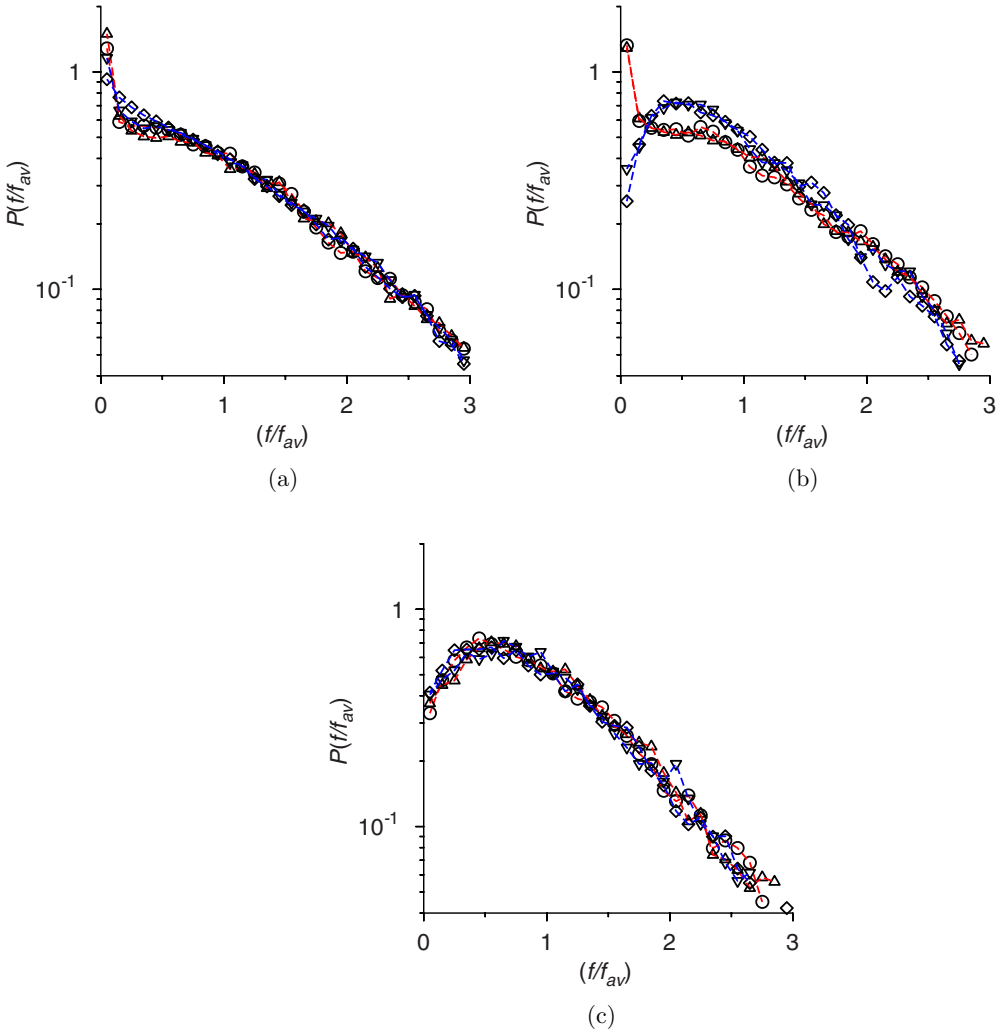

FIG. 8. The probability distribution for the contact force $P(f/f_{\rm av})$ as a function of $(f/f_{\rm av})$ for (a) a static layer at $\theta = 19.5^\circ$, (b) layered flow at $\theta = 19.6^\circ$, and (c) Bagnold flow at $\theta = 19.9^\circ$. The layer height is about 65 particle diameters, and the symbols show the distributions in intervals of height 4 particle diameters at heights of 6 ($\circ$, red), 26 ($\triangle$, red), 46 (∇, blue), and 62 ($\diamond$, blue) particle diameters from the base.

cessation is shown in Fig. 10(a). The two distinct regimes, the layered flow regime and the Bagnold flow regime, are visible in Fig. 10(a) for both the linear and Hertzian models. There is a relatively gradual increase in the velocity of the center of mass in the layered flow regime within the range of angles 19.55–19.75° for the linear model, and $\bar{v}_x^{\rm c.m.}$ appears to increase roughly proportional to the height of the flow. When the angle of inclination is greater than 19.8°, the system transitions to a Bagnold flow, where the mean velocity is proportional to $h^{3/2}$, as indicated by Eq. (8). These two regimes are also clearly observed for the Hertzian contact model for a layer of height about 70 particle diameters. Here, the layered flow regimes extends over a larger range 19°–20° in the angle of inclination, and then there is a transition to Bagnold flow when the angle of inclination is 20.1° or higher. There is a distinct shift in $\bar{v}_x^{\rm c.m.}$ upon transition from the layered flow to the Bagnold flow regime, and the height dependence of $\bar{v}_x^{\rm c.m.}$ is consistent with the $h^{3/2}$ scaling expected for the Bagnold profile.

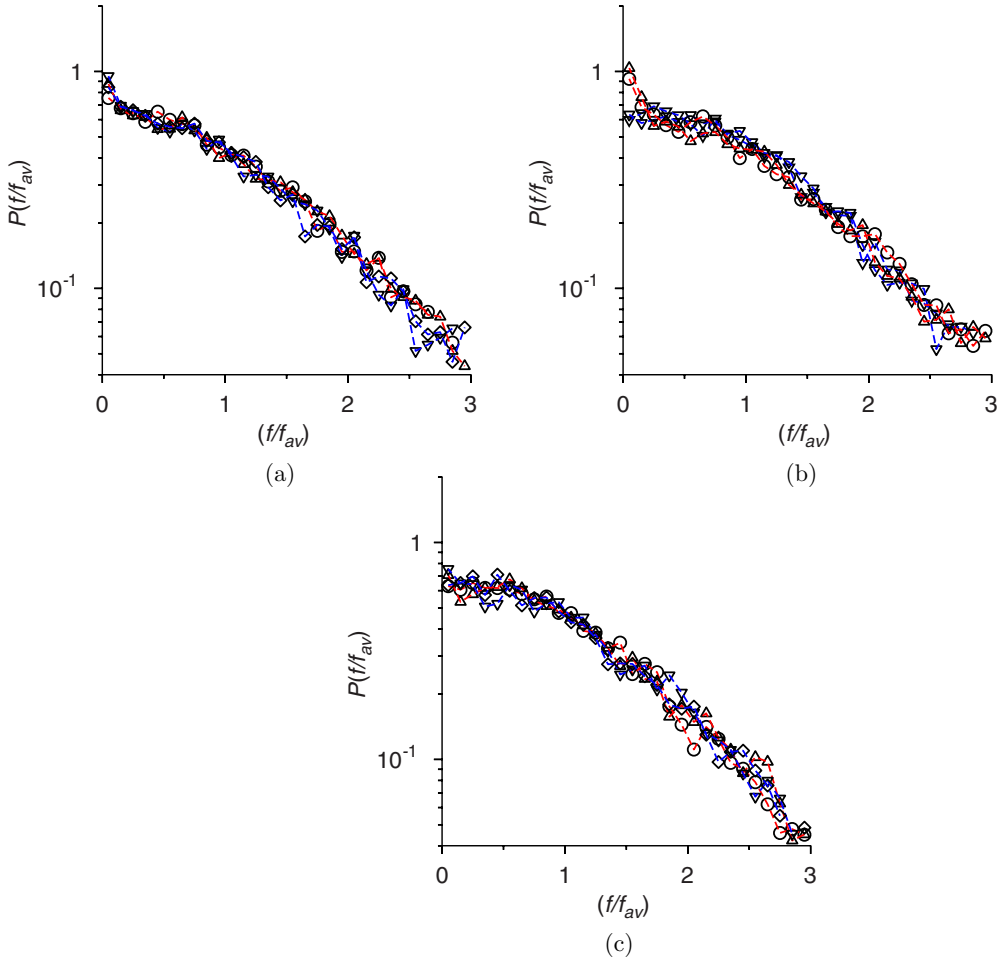

FIG. 9. The probability distribution of the contact force $P(f/f_{\rm av})$ as a function of $(f/f_{\rm av})$ for (a) a static layer at $\theta = 19^\circ$, (b) layered flow at $\theta = 19.5^\circ$, and (c) Bagnold flow at $\theta = 20.5^\circ$. The layer height is about 70 particle diameters, and the symbols show the distributions in intervals of height 4 particle diameters at heights of 6 (○, red), 26 (△, red), 46 (▽, blue), and 62 (◇, blue) particle diameters from the base.

The root mean square of the velocity fluctuations in the x and z directions, $\sqrt{\overline{(v_x^{\rm c.m.\prime})^2}}$ and $\sqrt{\overline{(v_z^{\rm c.m.\prime})^2}}$ [Eq. (5)], scaled by the average velocity of the center of mass $\bar{v}_x^{\rm c.m.}$, are shown in Figs. 10(b) and 10(c). There is a sharp increase in the scaled root mean square of the fluctuations in the Bagnold flow regime as the angle of inclination decreases until about 19.8° for the linear model and about 20° for the Hertzian models. Below this angle, when the system is in the layered flow regime (19.55°–19.75° for the linear model and 19°–20° for the Hertzian model), the root mean square of the velocity fluctuations (scaled by the velocity of the center of mass) show very little variation with the angle of inclination. The streamwise root mean square velocity, when scaled by the average velocity, is about 8%, while the scaled cross-stream root mean square velocity is about 12%. A similar variation is observed for the Hertzian contact model, where the scaled root mean square fluctuations increase sharply in the Bagnold flow region as the angle of inclination is decreased to 20°, and then are approximately invariant with angle of inclination in the layered flow regime when the angle of inclination is 19°–20°. Thus, there are distinct qualitative characteristics

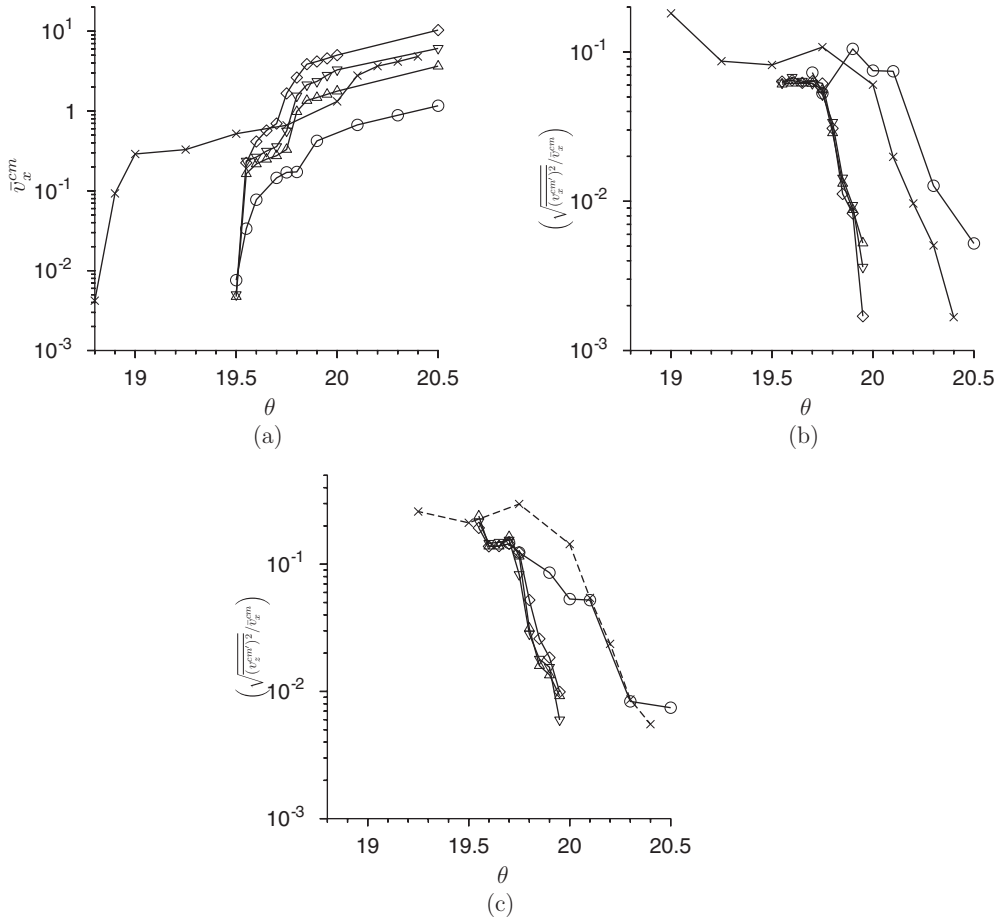

FIG. 10. The velocity of the center of mass $\bar{v}_x^{\text{c.m.}}$ (a), the scaled root mean square of the fluctuations in the streamwise velocity (b), and base-normal velocity (c) as a function of angle of inclination for the linear contact model with scaled particle stiffness 10^6 and layer height about 35 ($\circ$), 70 ($\triangle$), 100 (∇), and 140 ($\diamond$) and for the Hertzian contact model with scaled particle stiffness 10^6 and layer height 70 ($\times$).

of both the velocity of the center of mass and the velocity fluctuations in the layered flow regime close to cessation, which are very different from those in the Bagnold flow regime.

These fluctuations in the velocity of the center of mass are not random but have a regular sinusoidal variation in time, as shown in Fig. 11. Here, the instantaneous value of the fluctuating velocities of the center of mass, $v_x^{\text{c.m.}'}$ and $v_z^{\text{c.m.}'}$, are shown as a function of time scaled by the collision time τ_c. The fluctuating velocities for four different angles of inclination are shown in Fig. 11; all of these have zero mean, and the results for the different angles are vertically displaced for clarity. Figure 11(a) clearly shows that there are sinusoidal oscillations of a single frequency in the fluctuations in the velocities of the center of mass in the layered flow regime, between angles 19.55° and 19.75° for the linear model. The fluctuations in the streamwise and cross-stream velocities are anticorrelated; that is, the streamwise velocity passes through a maximum when the cross-stream velocity passes through a minimum, and vice versa. This implies that when the streamwise velocity is lower than average, there is an upward cross-stream velocity fluctuation, and when the streamwise velocity is higher than average, there is a downward cross-stream velocity fluctuation, resulting in periodic expansion and contraction of the flow. This is because a region decelerating in the streamwise direction has to expand to conserve volume, and the expansion is

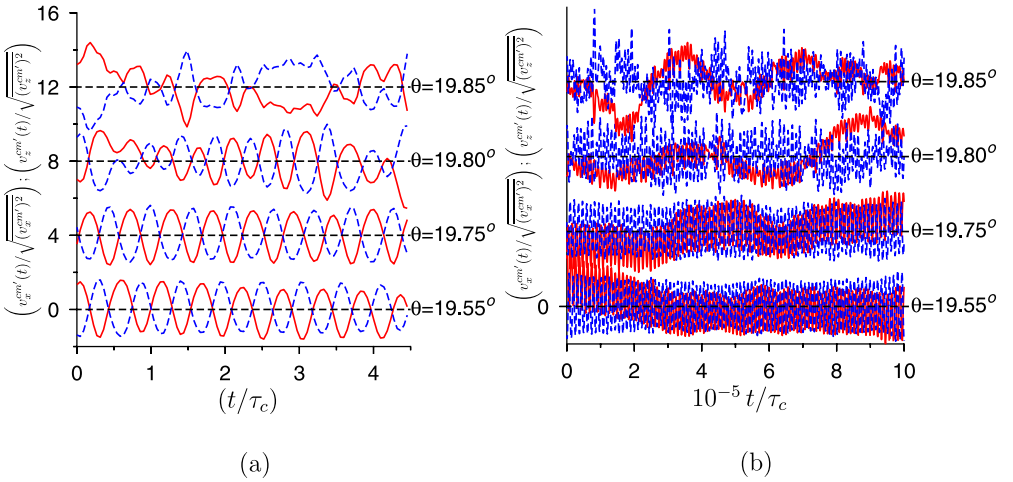

FIG. 11. The time series of the fluctuation in the velocity of the center of mass in the x direction (red, solid line) and z direction (blue, dashed line) for the short time series (a) and the long time series (b) for different angles of inclination for a layer of height about 70 particle diameters and the linear particle contact model with scaled particle stiffness 10^6.

upward due to the impenetrable base. When the angle of inclination is increased to 19.8° and the system is in the Bagnold flow regime, the sinusoidal variations disappear and the fluctuations are random in nature. Though there are some variations in the fluctuating velocity for long times, as shown in Fig. 11(b), the amplitude of the short-time fluctuations in Fig. 11(a) is larger than the amplitude of the long-time drift.

The velocity fluctuations are also observed for different heights, as shown in Fig. 12(a). There is a definite increase in the time period τ_o of the fluctuations as the height is increased, but clear anticorrelated fluctuations in the streamwise and cross-stream velocities are observed for all heights. These fluctuations are also observed for different contact models, and for different particle stiffness,

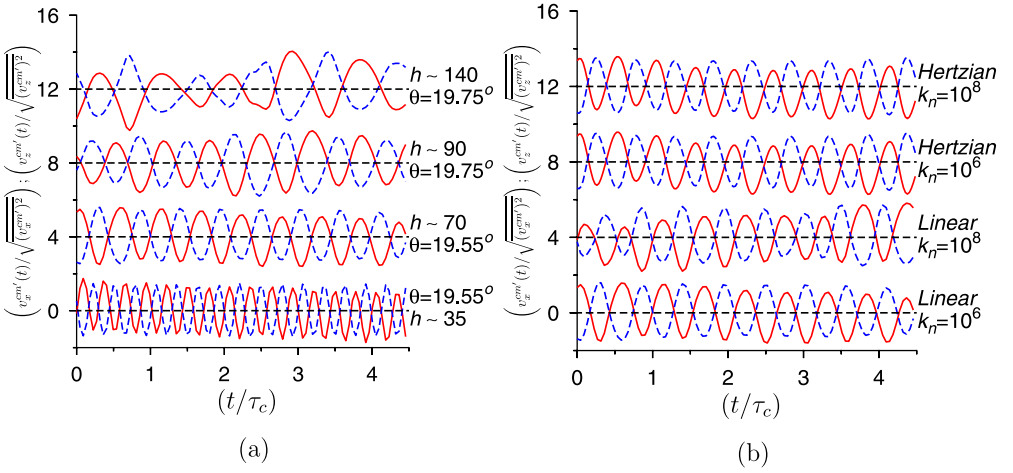

FIG. 12. The time series of the fluctuation in the velocity of the center of mass in the x direction (red, solid line) and z direction (blue, dashed line) for different layer heights for the linear model with $k_n = 10^6$ (a) and for different particle models and spring stiffness for layer height about 70 (b).

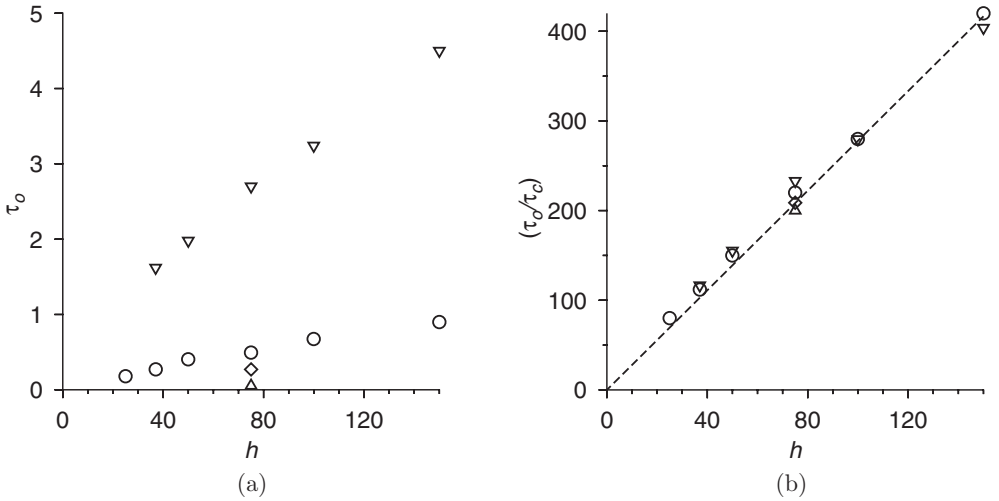

FIG. 13. The period of the oscillations for the layered flow as a function of the height of the flowing layer where the linear contact model is used for particle interactions with scaled particle stiffness $k_n = 10^6$ (○) and 10^8(△), and where the Hertzian contact model is used for the particle interactions with scaled particle stiffness $k_n = 10^6$ (▽) and 10^8 (◇). The period of oscillation is scaled by $\sqrt{d/g}$ in panel (a), and by the collision time $[(\pi(2k_n/m - \gamma_n^2/4)^{-1/2})$ for the linear model and $(\pi(2k_n/m - \gamma_n^2/4)^{-1/2}\bar{\delta}_n^{-1/4})$ for the Hertzian model] in panel (b).

as shown in Fig. 12(b). Simulations have also been carried out to examine whether these oscillations depend on system size. The size of the simulations have been increased by a factor of 2 in both the streamwise and the spanwise directions for both contact models and for different heights, and it is found that there is no change in the nature or the time period of the oscillations. Thus, the sinusoidal variation in the velocity fluctuations of the center-of-mass is a property of the layered flow and does not depend on contact model, flow height, or system size.

The variation of the time period of oscillations τ_o is shown as a function of layer height for the linear and Hertzian contact models in Fig. 13. Different layer heights are considered for the linear contact model with two different values of the particle stiffness, while one height is considered for the Hertzian contact model with two different values of the particle stiffness to examine how the contact model affects the period of oscillations. When scaled by $\sqrt{d/g}$, Fig. 13(a) shows that there is a significant variation in the period of oscillation. However, when the period of oscillation is scaled by the contact time τ_c, Fig. 13(b) shows that all the date collapses on to a single curve. The period of oscillation seems to increase linearly with height for the range of heights considered here.

VI. CESSATION OF FLOW

The dynamics of flow cessation, when the angle of inclination of a flowing layer of particles initially at 22°, is instantaneously decreased to different angles above and below the cessation angle, is examined in this section. In the simulations, the angle of inclination is set equal to 22°, and the simulation is run until steady state is attained. The angle of inclination is then decreased instantaneously to a lower value θ_s, which could be above or below the angle for flow cessation, and the decrease in the average velocity with time is determined. The particles come to rest when the angle of inclination is below that for flow cessation, and the rate of decrease is faster for a lower final angle θ_s. When θ_s is greater than the angle for flow cessation, the velocity decreases and reaches a final value at steady state which is lower than the initial value for 22°. The qualitative nature of the decrease in the velocity is examined as a function of the final angle θ_s, the layer height, the particle stiffness, and the contact model. The dynamics of flow cessation is qualitatively similar for

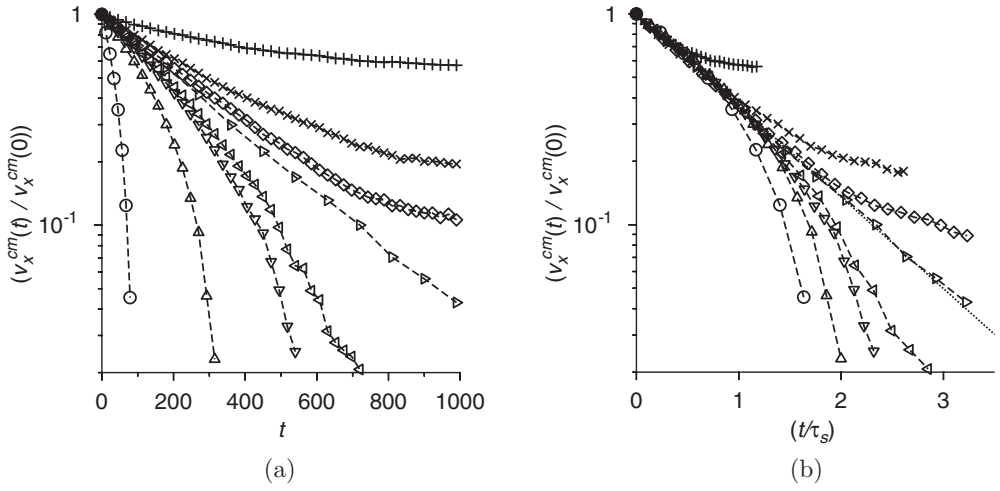

FIG. 14. The decrease in the average velocity $v_x^{\text{c.m.}}$ [Eq. (2)] as a function of time when the angle of inclination of a layer of height about 70 particle diameters, initially flowing at inclination angle 22°, is instantaneously decreased to 10° (○), 18° (△), 19° (▽), 19.2° (◁), 19.5 (▷), 19.7° (◇), 20.0° (×), and 21.0° (+). The velocity is plotted as a function of time in panel (a) and as a function of (t/τ_s) in panel (b). The dotted line in panel (b) shows the curve $\exp(-t/\tau_s)$.

disordered and ordered flows. The flow cessation of a disordered flow is discussed in detail, while the important results for the ordered flow are briefly presented.

The decrease in the average streamwise velocity of the center of mass, $v_x^{\text{c.m.}}$ [Eq. (2)], is shown as a function of time for different decrements in the angle of inclination in Fig. 14. Here, the layer height is about 70 particle diameters, the linear contact model is used, and the particle stiffness is 10^6. In Fig. 14(a), the ratio of the instantaneous velocity and the initial velocity is shown as a function of time. When the angle of inclination is decreased to 10°, there is a rapid decrease by about two orders of magnitude within about 100 time units. The time for decrease increases as the final angle of inclination increases up to about 19.5°, the angle for cessation of flow. When the angle increases to 19.7°, the flow velocity does not decrease monotonically but tends to a finite value in the long time limit. As the final angle of inclination increases to 20° and 21°, the final velocity increases. Though this behavior is intuitively expected, deeper insight is obtained by scaling the time axis by an angle-dependent cessation time τ_s in Fig. 14(b). Here, it is observed that the initial decrease of the velocity collapses on to the same exponential curve for all angles of inclination, including those angles where the final state is flowing. When the final angle is less than 19.5°, there is a two-stage decrease in the mean velocity, the initial exponential decrease, and a second faster-than-exponential decrease for $t > \tau_s$. When the angle of inclination is greater than 19.5°, the initial decrease is followed by a plateau to the steady velocity at that angle. At the angle of 19.5°, where there is flow cessation, the decrease in the mean velocity appears to be exponential with a single relaxation time τ_s.

Though the decrease of the average velocity with time exhibits a self-similar behavior when the time is scaled by the time constant time τ_s, the velocity profiles do not decrease in a self-similar manner. This is shown in Fig. 15, where the velocity profiles at equal values of (t/τ_s) are shown for different final stopping angles θ_s. When the final angle is 0, there is a rapid decline in the velocity profile to zero at the bottom, and this region of zero velocity progresses upward until the flow stops. As the final angle θ_s increases, the form of the velocity profile at intermediate time changes. There is a more uniform decrease in the velocity throughout the height when θ_s is 15° or greater. When the angle of inclination is 20°, which is greater than the angle of cessation, the initial decrease is exponential, but the velocity profiles tends to a steady state profile 20° for $(t/\tau_s) > 1$. Therefore, the

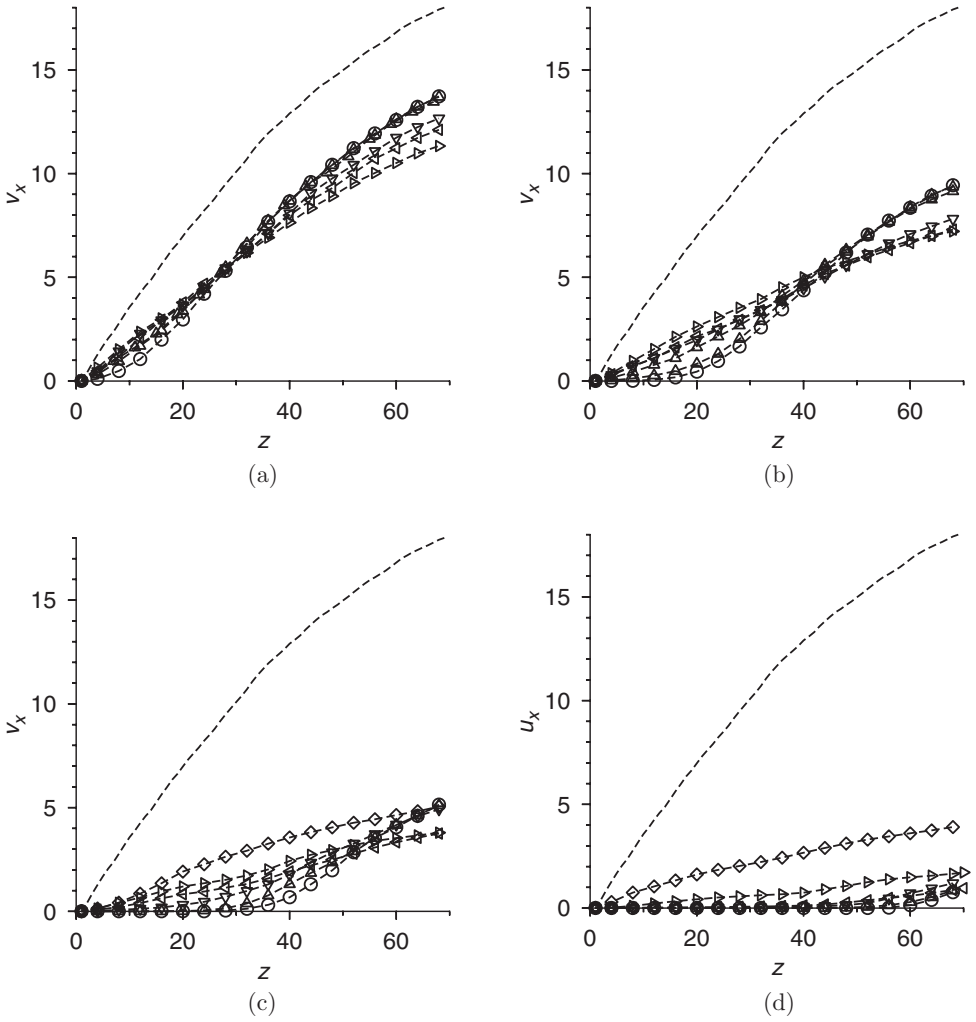

FIG. 15. The velocity profiles at different time instants $(t/\tau_s) = 0.5$ (a), 1.0 (b), 1.5 (c), and 2.0 (d) for a disordered flow when the angle of inclination of a layer of height 70, with initial angle of inclination 22°, is instantaneously decreased to 0° (○), 10° (△), 15° (▽), 18° (◁), 19° (▷), and 20.0° (◇). The dashed line shows the steady-state velocity profile for 22° at $t = 0$.

velocity profiles during flow cessation do depend on the final angle θ_s, though the initial decrease in the center-of-mass velocity is self-similar.

The relationship between the strain rate and the granular temperature during flow cessation is shown in Fig. 16 for different cessation angles. When compared with the velocity profiles in Fig. 15, it is observed that there are two distinct qualitative features. Where there is no flow at the bottom, the ratio decreases to zero. Where there is flow at the top, the ratio $[(dv_x/dz)^2/T]$ has a finite value which is independent of height, independent of time, and dependent only on the angle of inclination. The transition in the value of $[(dv_x/dz)^2/T]$ between the flowing and static regions takes place over a distance of about 5–8 particle diameters. The constant value of $[(dv_x/dz)^2/T]$ is predicted by kinetic models for granular flows, which posit a local balance between the production of energy due to shear and the dissipation due to inelastic collisions. The implicit assumption here is that the inverse of the strain rate provides the only timescale in the problem. Thus, the flowing region seems to be well described by the hard-particle approximation. The transition zone of 5–8 particle

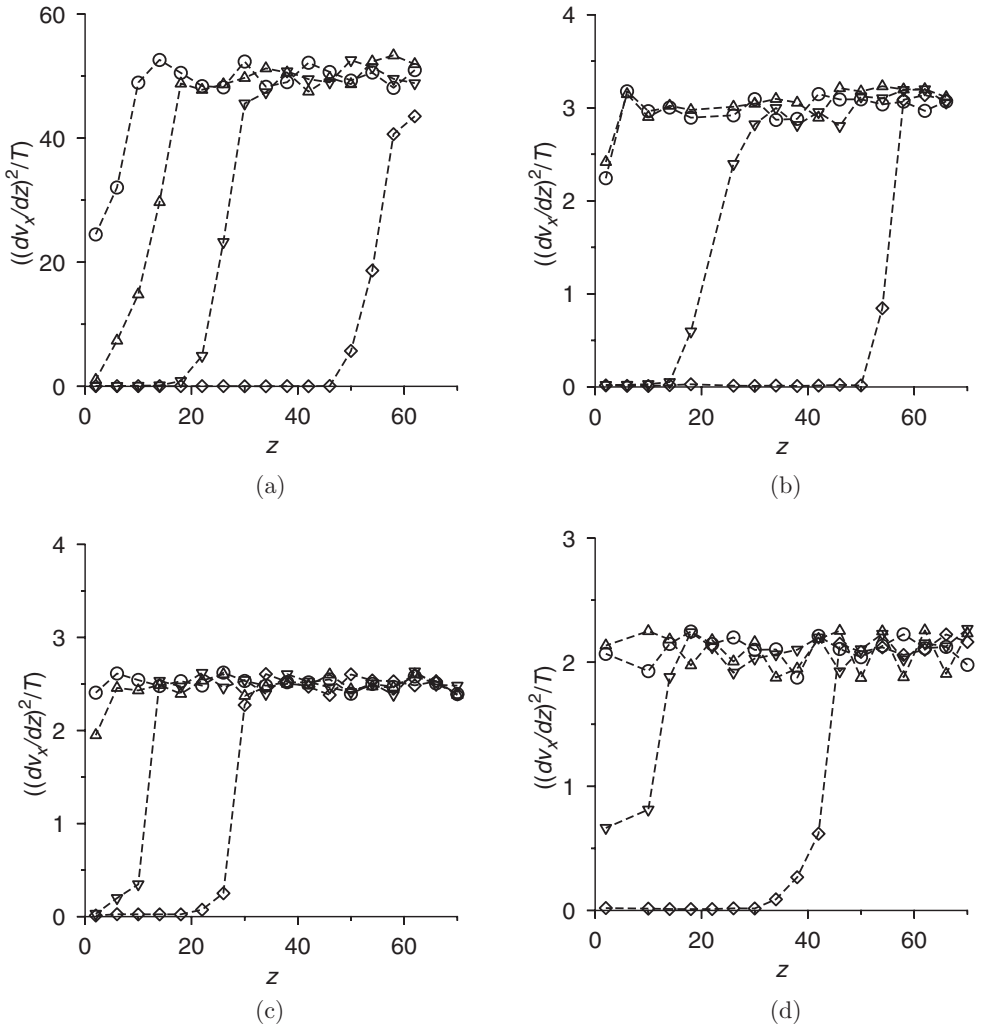

FIG. 16. The ratio of the square of the strain rate and the granular temperature for $(t/\tau_s) = 0.5$ (○), $(t/\tau_s) = 1.0$ (△), $(t/\tau_s) = 1.5$ (▽), and $(t/\tau_s) = 2.0$ (◇) during the cessation of the flow down an inclined plane when the initial angle of the steady flow is 22°, and the angle of inclination is instantaneously decreased to 0° (a), 10° (b), 15° (c), and 18° (d).

diameters over which the transition takes place correlates well with the presence of a conduction boundary layer of thickness 5–8 particle diameters for steady flows over irregular boundaries [61]. The ratio of the square of the strain rate and the granular temperature in the flowing region does have a definite dependence on the angle of inclination. This ratio decreases as the final angle of inclination θ_s increases, implying that the agitation of the particles at fixed strain rate decreases as the final angle of inclination decreases.

The characteristic time for the initial exponential decrease of the center-of-mass velocity, τ_s, is shown as a function of θ_s in Fig. 17(a). The value of τ_s is determined by fitting a straight line to the initial decay of the velocity in the semilog graph shown in Fig. 14(a), and determining the time at which this line intersects $[v_x^{\text{c.m.}}(t)/v_x^{\text{c.m.}}(0)] = e^{-1}$, where e is the base of the natural logarithm. Instead of τ_s, Fig. 17 shows the ratio $(\tau_s/h^{3/2})$, since this results in a collapse of the data. As intuitively expected, τ_s increases as the final angle θ_s increases, and it appears to diverge

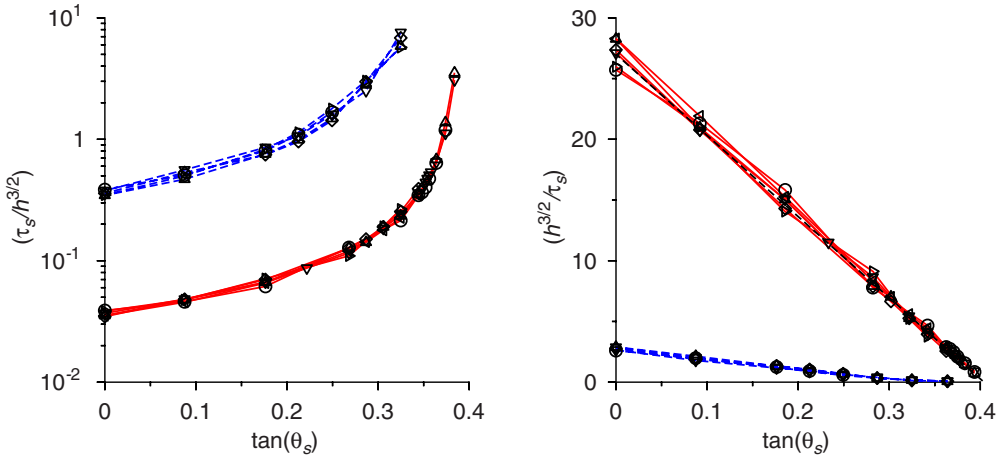

FIG. 17. The variation of $(\tau_s/h^{3/2})$ (a) and $(h^{3/2}/\tau_s)$ (b) as a function of tan (θ_s) for a disordered flow (solid red line) and ordered flow (dashed blue line) for the linear contact model for $k_n = 10^6$ and $h = 37$ ($\circ$), $h = 48$ ($\triangle$), $h = 75$ (∇), and $h = 100$ ($\diamond$), for the linear contact model for $k_n = 10^8$ and $h = 75$ ($\triangleleft$), and for the Hertzian model for $k_n = 10^6$ and $h = 75$ ($\triangleright$).

as θ_s approaches the initial angle 22°. In Fig. 17(b), the inverse $(h^{3/2}/\tau_s)$ is plotted as a function of tan (θ_s). This figure shows that $(h^{3/2}/\tau_s)$ decreases linearly with tan (θ_s), and it appears to extrapolate to zero at $\theta = 22°$, the initial angle for the steady flow. Moreover, the results for different particle contact models and different particle stiffnesses in Fig. 17 show that the cessation time τ_s increases proportional to $h^{3/2}$ and is independent of the particle stiffness or the contact model.

All the qualitative features of the flow cessation for an ordered flow are identical to those for a disordered flow. The initial exponential decrease of the velocity of the center of mass is observed for a disordered flow as well. When scaled by the characteristic time τ_s for flow cessation, the initial decrease of the velocity is found to be universal. When θ_s is lower than the flow cessation angle, there is a faster decrease of the velocity for $(t/\tau_s) \gtrsim 1$. When θ_s is higher than the flow angle, the flow reaches the final steady velocity in the long time limit. Though the decrease of the velocity of the center of mass is universal when time is scaled by the characteristic cessation time, the velocity profiles are not universal. For low values of θ_s, the velocity decreases faster at the bottom and more slowly at the top, whereas for high values of θ_s, there is relatively uniform deceleration throughout the height. The temperature is proportional to the square of the strain rate in the flowing region for the ordered state as well. The cessation time τ_s and its inverse are shown by the blue dashed lines in Fig. 17 for the ordered state. The characteristic cessation time for an ordered flow is numerically about one order of magnitude higher for a disordered flow. However, all the qualitative features of τ_s are the same. Figure 17 shows that τ_s is proportional to $h^{3/2}$ and is independent of the particle contact model and the particle stiffness, for both ordered and disordered flows. When extrapolated, the characteristic cessation time for ordered and disordered flows appears to diverge at the angle $\theta_s = 22°$, which is the initial angle of inclination, as required for consistency.

There is a subtle difference between the characteristic time τ_s for ordered and disordered flows. For a disordered flow, the inverse of the characteristic cessation time τ_s^{-1} decreases linearly with the tangent of the angle of inclination. For an ordered flow, the decrease is not linear, and τ_s^{-1} appears to decrease with zero slope at $\theta_s = 22°$. It should be noted that the time τ_s becomes very large for an ordered flow for $\theta \to \theta_s$, and the required time period is too large to simulate for $\theta_s > 20°$. Despite this limitation, the results in Fig. 17(b) clearly show that the decrease of τ_s^{-1} is not linear when the

angle of inclination is close to θ_s. This subtle difference, and its connection to the variation in the Bagnold coefficient near flow cessation, is a subject for further study.

VII. CONCLUSIONS

A. Bagnold flow

In this study, we have examined the validity of Bagnold law and the nature of the velocity profile as the angle of inclination is decreased very close to the angle for flow cessation. The results show that the mean velocity profiles are well described by the Bagnold law even when the angle of inclination exceeds the angle of cessation by not more than about 0.5° for a disordered flow for the linear contact model, when the layer height exceeds about 48 particle diameters. This implies the flow is in the Bagnold regime even when the ratio of shear and normal stresses is 2.5% higher than that for dynamical arrest. For a disordered flow for the Hertzian contact model, Bagnold law applies when the angle of inclination is 1° higher than the angle for flow cessation. The Bagnold profile for the velocity field and the characteristic linear increase in the temperature with depth are observed even when the coordination number is greater than 2. Though the Bagnold coefficient increases by two orders of magnitude when the angle of inclination is decreased by about 2°, the velocity profile is found to be quantitatively described by the Bagnold profile. This property of the dense granular flow down an inclined plane is found to be independent of the flow height, the particle stiffness, or the particle contact model. This remarkable robustness of the Bagnold law even very close to cessation confirms that constitutive relations based on the hard-particle approximation are valid even in regions where the ratio of the shear and normal stresses is close to that for flow arrest.

Flow cessation for an ordered flow is different from that for a disordered flow. Here, the transition occurs from a Bagnold regime to a plug flow as the angle of inclination is decreased. In the plug flow regime, there is a sliding region at the base of thickness a few particle diameters, which supports a plug above with no internal shearing. The transition between the plug flow and the Bagnold flow is even sharper than that for the disordered flow. In the simulations, the transition is observed to occur when the angle of inclination is decreased by 0.05°, independent of layer height, particle interaction model, or particle stiffness. There is no other flow regime discernible between the Bagnold regime and the plug flow regime for an ordered flow. Thus, ordered flowing states with internal shearing appear to always be in the Bagnold regime.

There is a significant difference in the variation of the Bagnold constant in ordered and disordered flows close to cessation. In the case of a disordered flow, the Bagnold coefficients B_{xz} and B_{zz} appear to diverge, and the inverse of the Bagnold coefficients B_{xz}^{-1} and B_{zz}^{-1} appears to continuously decrease to zero, suggesting that the transition is continuous. The decrease to zero of B_{xz}^{-1} and B_{zz}^{-1} is interrupted by a transition to the layered flow regime close to cessation, discussed next. However, there is a large decrease in B_{xz}^{-1} and B_{zz}^{-1}, by about two orders of magnitude, when the angle of inclination decreases by about 2°. In the case of an ordered flow, the change in the Bagnold coefficient is discontinuous. The inverse of the Bagnold coefficients, B_{xz}^{-1} and B_{zz}^{-1}, decrease by a factor of about 1.5 when the angle of inclination decreases from 22° to 16°, and then they discontinuously decrease to zero when the angle of inclination is further decreased by 0.05°. Thus, the cessation transition for ordered and disordered flows appear to belong to different universality classes.

A similarity between the cessation transition for a disordered flow and phase transitions in equilibrium systems is illustrated in Fig. 10, where the scaled root mean square of the velocity fluctuations are shown as a function of the angle of inclination. The sharp increase of the root mean square velocity in Fig. 10 is reminiscent of the power law increase in the fluctuation amplitude in the vicinity of a critical point. For example, near the critical point for a binary fluid system, the amplitude of the fluctuations increases as $(T - T_c)^{-\alpha}$, where T is the temperature, T_c is the critical temperature, and α is a positive "critical exponent." If the angle of inclination is akin to T, the divergence of the root mean square velocities is suggestive of the divergence near a critical point. When the transition is close to the critical point but still first order, the divergence is truncated

beyond a certain amplitude. The constant value of the root mean square velocities in the layered flow regime in Fig. 10 is reminiscent of the cutoff of the divergence. Thus, there are similarities between the nature of the fluctuations near flow cessation and phase transition in an equilibrium system, but this requires deeper study.

This distinction in the universality class of the transition has important consequences for the modeling of real granular flows, which often simultaneously contain static and flowing regions. A continuous increase in B_{xz}^{-1} and B_{zz}^{-1} from zero implies that the strain rate continuously increases from zero at the interface between static and flowing regions. A discontinuous change in B_{xz}^{-1} and B_{zz}^{-1} implies that the strain rate changes discontinuously at the boundary between the static and flowing regions. In both cases, it bears reiteration that the applicability of the Bagnold profile implies that the material timescales are not relevant and the only timescale in the problem is the inverse of the strain rate.

B. Layered flow

For the disordered flow, for angles of inclination between the Bagnold flow and flow cessation, there is a narrow range of angles for which a distinct layered flow is observed. The range of angles is very small, less than 0.5° for the linear contact model and about 1° for the Hertzian contact model. The flow is very different from the Bagnold flow and consists of a region of about 30 particle diameters with a larger strain rate atop a region with a lower shear rate down to the base. A salient result is that the transition from the Bagnold flow to the layered flow is abrupt, as shown in Figs. 2, 3, and 4, for example. The transition takes place when the angle of inclination is increased by 0.05°. It may be possible to model the layered flow using a nonlocal model with correlation length larger than the system size. However, the transition to a layered flow cannot be predicted if the correlation length increases continuously as the angle of inclination is increased. It is necessary to postulate a discontinuous jump in the correlation length in order to predict such a transition.

The dynamics in the layered flow regime is intriguing. One would have expected the flow to transition to an intermittent avalanching regime when the angle of inclination is too small for a steady flow but still large enough that the layer is not stationary. Instead, regular sinusoidal oscillations are observed in the streamwise and cross-stream velocities of the center of mass. The amplitude of the streamwise velocity oscillations is about 8% of the average velocity, while that of the cross-stream velocity oscillations is about 12% of the average velocity. The amplitude of the oscillations, when scaled by the velocity of the center of mass, is approximately a constant in the layered flow regime. This is in contrast to the Bagnold regime, where the amplitude of the fluctuations increases sharply as the angle of inclination is decreased near flow cessation. The time period of the oscillations τ_o does vary with layer height, the contact model, and the particle stiffness. An important finding is that τ_o is proportional to the collision time, that is, the period of a collision between two particles. The comparison has to be made carefully, because the collision time is independent of precollisional velocity for the linear contact model but does depend on the precollisional velocity for the Hertzian contact model. Here, we have used an average collision time based on the average overlap between the particles for the Hertzian contact model. When the time period of the sinusoidal oscillations is scaled by the collision time calculated in this manner, it is found that the ratio is independent of the contact model or the particle stiffness, and it depends only on the height of the flowing layer.

The dynamics of the layered flow is therefore dependent on the particle interaction time, which is a material timescale. For deep flows in the layered flow regime, the thickness of the upper shearing zone is approximately a constant, independent of the total height. The simulations show that the two regions have different force distributions. The force distribution in the shearing layer on top is similar to that for the flowing state, while that in the low shear region at the bottom is similar to that for a static layer. Thus, the distinction between the upper and lower layers is not just kinematic, but there are dynamical differences in the contact force distributions.

This linear profile for a layered flow is similar to what is observed in the flow over a heap or an erodible bad. While the similarity in the velocity profiles may just be superficial, it is also possible that there is a deeper connection. In the flow over a heap, the angle of inclination of the top flowing layer is close to the angle of repose, which would correspond to the layered flow regime in the flow over an inclined plane. Thus, the flow may be dynamically aligning close to the angle for cessation, so that the flow is always in the layered regime. The possibility of such a connection requires further research.

Another important observation in the present study is the near discontinuous increase in the coordination number at flow cessation. This observation has to be interpreted with care. Even after cessation of flow, it is observed in the simulations that the coordination number does not increase to the expected isostatic value of 4, due to long-lasting vibrations at the contacts which lead to instantaneous formation and breaking of contacts. It is necessary to artificially dampen these vibrations in order to attain a static state with the coordination number near 4. In the flowing state, it is observed that even when there is a static layer at the bottom, the stress exerted by the flow on top results in the mobilization of contacts in the static layer and the consequent decrease in the coordination number. Since the particle stiffness used here is significantly smaller than that for real particles such as sand and glass, this mobilization of contacts with high-frequency vibrations in a static layer is likely to be real effect.

C. Cessation of flow

The dynamics of the cessation of flow when the angle of inclination is decreased exhibits some interesting features, which are common to ordered and disordered flows. In the simulations, a steady flow was set up with angle of inclination 22°, the angle of inclination was instantaneously decreased to a lower value θ_s, and the rate of decrease of the velocity was examined. The initial decay of the height-averaged velocity is found to follow an exponential decay with a relaxation time τ_s, followed by a faster decay if θ_s is below the angle for flow cessation. When θ_s is above the angle for flow cessation, the flow evolves to the steady profile for the angle of inclination θ_s, with an initial decay that is exponential. Though the height-averaged velocity is well approximated by an exponential decay, the velocity profiles do not collapse on to a universal profile for equal values of (t/τ_s), where t is the time elapsed since the reduction in the inclination angle.

At the early stages of flow deceleration when the departure from the initial velocity profile is not large, the momentum equation can be linearized in the departure from the initial profile, and the decay is expected to be exponential. Comparing Figs. 14, 15, and 16, it is observed that the decay is exponential when there is shearing throughout the height of the layer, and the granular temperature is proportional to the square of the strain rate throughout the height. The faster-than-exponential decay seems to start when there is a static region at the bottom with no shear supporting a flowing layer at the top. In this case, the linearization approximation is not valid, and the decrease in the velocity profile is expected to be faster than exponential because the deceleration is faster as the thickness of the shearing region decreases.

Even though the velocity profile is not self-similar, there are several aspects of the flow cessation process that can be described by the hard-particle approximation. The ratio of the square of the strain rate and the temperature, $[(dv_x/dz)^2/T]$, is independent of height in the flowing region. In contrast, the ratio decreases in the static region at the bottom which appears at the late stages of flow cessation. The relaxation time τ_s for the exponential relaxation is independent of the particle stiffness, and it scales proportionally to $h^{3/2}$ with the layer height. This is the expected scaling if the Bagnold law is used for the stress in the bulk [72]. Thus, all of the qualitative features of the initial decay of the velocity profile are consistent with the hard particle model for a dense granular flow.

ACKNOWLEDGMENTS

The authors would like to thank the Department of Science and Technology, Government of India. This research was supported by the J. R. D. Tata Memorial Trust. V.K. would like to thank the

Kavli Institute of Theoretical Physics, University of California, Santa Barbara, USA, for hospitality. This research was supported in part by the National Science Foundation under Grant No. NSF PHY17-48958.

[1] B. J. Alder and T. E. Wainwright, Decay of the velocity autocorrelation function, Phys. Rev. A **1**, 18 (1970).
[2] W. G. Hoover and F. H. Ree, Melting transition and communal entropy for hard spheres, J. Chem. Phys. **49**, 3609 (1968).
[3] S. Torquato, Nearest-neighbor statistics for packings of hard spheres and disks, Phys. Rev. E **51**, 3170 (1995).
[4] V. S. Kumar and V. Kumaran, Voronoi cell volume distribution and configurational entropy of hard spheres, J. Chem. Phys. **123**, 114501 (2005).
[5] R. Bagnold, Experiments on a gravity-free dispersion of large solid spheres in a Newtonian fluid under shear, Proc. R. Soc. London, Ser. A **225**, 49 (1954).
[6] R. Bagnold, The flow of cohesionless grains in fluids, Proc. R. Soc. London, Ser. A **249**, 235 (1954).
[7] K. A. Reddy and V. Kumaran, Applicability of constitutive relations from kinetic theory for dense granular flows, Phys. Rev. E **76**, 061305 (2007).
[8] K. A. Reddy and V. Kumaran, Dense granular flow down an inclined plane: A comparison between the hard particle model and soft particle simulations, Phys. Fluids **22**, 113302 (2010).
[9] C. Campbell, Clusters in dense-inertial granular flows, J. Fluid Mech. **687**, 341 (2011).
[10] S. Bharathraj and V. Kumaran, Effect of particle stiffness on contact rheology and dynamics in a dense granular flow, Phys. Rev. E **97**, 012902 (2018).
[11] S. Chapman and T. G. Cowling, *The Mathematical Theory of Non-Uniform Gases*, Cambridge Mathematical Library (Cambridge University Press, Cambridge, UK, 1991).
[12] I. Goldhirsch and G. Zanetti, Clustering Instability in Dissipative Gases, Phys. Rev. Lett. **70**, 1619 (1993).
[13] J. J. Brey, J. W. Dufty, C.-S. Kim, and A. Santos, Hydrodynamics for granular flow at low density, Phys. Rev. E **58**, 4638 (1998).
[14] J. J. Brey, M. J. Ruiz-Montero, and D. Cubero, Homogeneous cooling state of a low-density granular flow, Phys. Rev. E **54**, 3664 (1996).
[15] J. J. Brey, M. J. Ruiz-Montero, and D. Cubero, Origin of density clustering in a freely evolving granular gas, Phys. Rev. E **60**, 3150 (1999).
[16] J. J. Brey and J. W. Dufty, Hydrodynamic modes for a granular gas from kinetic theory, Phys. Rev. E **72**, 011303 (2005).
[17] J. Dufty, A. Baskaran, and J. J. Brey, Linear response and hydrodynamics for granular fluids, Phys. Rev. E **77**, 031310 (2008).
[18] A. Baskaran, J. W. Dufty, and J. J. Brey, Transport coefficients for the hard-sphere granular fluid, Phys. Rev. E **77**, 031311 (2008).
[19] N. Khalil, V. Garzó, and A. Santos, Hydrodynamic Burnett equations for inelastic Maxwell models of granular gases, Phys. Rev. E **89**, 052201 (2014).
[20] P. K. Haff, Grain flow as a fluid-mechanical phenomenon, J. Fluid Mech. **134**, 401 (1983).
[21] C. K. K. Lun, S. B. Savage, D. J. Jeffrey, and N. Chepurniy, Kinetic theories for granular flow: Inelastic particles in Couette flow and slightly inelastic particles in a general flowfield, J. Fluid Mech. **140**, 223 (1984).
[22] C. K. K. Lun, Kinetic theory for the flow of dense, slightly inelastic, slightly rough spheres, J. Fluid Mech. **233**, 539 (1991).
[23] J. T. Jenkins and M. W. Richman, Grad's 13-moment system for a dense gas of inelastic particles, Arch. Ration. Mech. Anal. **87**, 355 (1985).
[24] N. Sela, I. Goldhirsch, and S. H. Noskowicz, Kinetic theoretical study of a simply sheared two dimensional granular gas to Burnett order, Phys. Fluids **8**, 2337 (1996).

[25] N. Sela and I. Goldhirsch, Hydrodynamic equations for rapid flows of smooth inelastic spheres, to Burnett order, J. Fluid Mech. **361**, 41 (1998).
[26] V. Kumaran, Constitutive relations and linear stability of a sheared granular flow, J. Fluid Mech. **506**, 1 (2004).
[27] V. Kumaran, The constitutive relation for the granular flow of rough particles, and its application to the flow down an inclined plane, J. Fluid Mech. **561**, 1 (2006).
[28] V. Garzo, Transport coefficients for an inelastic gas around uniform shear flow: Linear stability analysis, Phys. Rev. E **73**, 021304 (2006).
[29] A. Santos, V. Garzo, and J. W. Dufty, Inherent rheology of a granular fluid in uniform shear flow, Phys. Rev. E **69**, 061303 (2004).
[30] V. Kumaran, Temperature of a granular material "fluidized" by external vibrations, Phys. Rev. E **57**, 5660 (1998).
[31] J. J. Brey, M. J. Ruiz-Montero, and F. Moreno, Hydrodynamics of an open vibrated granular system, Phys. Rev. E **63**, 061305 (2001).
[32] J. J. Brey, M. J. Ruiz-Montero, F. Moreno, and R. Garcia-Rojo, Transversal inhomogeneities in dilute vibrofluidized granular fluids, Phys. Rev. E **65**, 061302 (2002).
[33] R. D. Wildman, J. M. Huntley, and D. J. Parker, Convection in Highly Fluidized Three-Dimensional Granular Beds, Phys. Rev. Lett. **86**, 3304 (2001).
[34] H. Viswanathan, N. A. Sheikh, R. D. Wildman, and J. M. Huntley, Convection in three-dimensional vibrofluidized granular beds, J. Fluid Mech. **682**, 185 (2011).
[35] B. Meerson, T. Poschel, and Y. Bromberg, Close-Packed Floating Clusters: Granular Hydrodynamics Beyond the Freezing Point? Phys. Rev. Lett. **91**, 024301 (2003).
[36] P. Eshuis, K. van der Weele, D. van der Meer, and D. Lohse, Granular Leidenfrost Effect: Experiment and Theory of Floating Particle Clusters, Phys. Rev. Lett. **95**, 258001 (2005).
[37] J. T. Jenkins, Dense shearing flows of inelastic disks, Phys. Fluids **18**, 103307 (2006).
[38] J. T. Jenkins, Dense inclined flows of inelastic spheres, Granular Matter **10**, 47 (2007).
[39] D. Berzi and J. T. Jenkins, Steady shearing flows of deformable inelastic spheres, Soft Matter **11**, 4799 (2015).
[40] V. Kumaran, Dynamics of dense sheared granular flows. Part i: Structure and diffusion, J. Fluid Mech. **632**, 109 (2009).
[41] V. Kumaran, Dynamics of dense sheared granular flows. Part ii: The relative velocity distribution, J. Fluid Mech. **632**, 145 (2009).
[42] A. V. Orpe, V. Kumaran, K. A. Reddy, and A. Kudrolli, Fast decay of the velocity autocorrelation function in dense shear flow of inelastic hard spheres, Europhys. Lett. **84**, 64003 (2008).
[43] V. Kumaran, Dynamics of a dilute sheared inelastic fluid. I. Hydrodynamic modes and velocity correlation functions, Phys. Rev. E **79**, 011301 (2009).
[44] V. Kumaran, Dynamics of a dilute sheared inelastic fluid. II. The effect of correlations, Phys. Rev. E **79**, 011302 (2009).
[45] L. E. Silbert, D. Ertas, G. S. Grest, T. C. Halsey, D. Levine, and S. J. Plimpton, Granular flow down an inclined plane: Bagnold scaling and rheology, Phys. Rev. E **64**, 051302 (2001).
[46] R. Brewster, L. E. Silbert, G. S. Grest, and A. J. Levine, Relationship between interparticle contact lifetimes and rheology in gravity-driven granular flows, Phys. Rev. E **77**, 061302 (2008).
[47] O. Pouliquen, Scaling laws in granular flows down rough inclined planes, Phys. Fluids **11**, 542 (1999).
[48] N. Mitarai and H. Nakanishi, Bagnold Scaling, Density Plateau, and Kinetic Theory Analysis of Dense Granular Flow, Phys. Rev. Lett. **94**, 128001 (2005).
[49] V. Kumaran, Dense granular flow down an inclined plane: From kinetic theory to granular dynamics, J. Fluid Mech. **599**, 121 (2008).
[50] V. Kumaran, Dense sheared granular flows, J. Fluid Mech. **756**, 555 (2014).
[51] L. E. Silbert, J. W. Landry, and G. S. Grest, Granular flow down a rough inclined plane: Transition between thin and thick piles, Phys. Fluids **15**, 1 (2003).
[52] G. D. R. MiDi, On dense granular flows, Eur. Phys. J. E **14**, 341 (2004).

[53] P. Jop, Y. Forterre, and O. Pouliquen, A constitutive law for dense granular flows, Nature (London) **441**, 727 (2006).
[54] P.-Y. Lagree, L. Staron, and S. Popinet, The granular column collapse as a continuum: Validity of a two-dimensional Navier-Stokes model with a μ(i) rheology, J. Fluid Mech. **686**, 378 (2011).
[55] A. Schofield and P. Wroth, *Critical State Soil Mechanics* (McGraw-Hill, New York, 1968).
[56] P. Jop, Rheological properties of dense granular flows, C. R. Phys. **16**, 62 (2015).
[57] T. Barker and J. M. N. T. Gray, Partial regularisation of the incompressible μ(i) rheology for granular flow, J. Fluid Mech. **828**, 5 (2017).
[58] K. Kamrin and D. L. Henann, Nonlocal modeling of granular flows down inclines, Soft Matter **11**, 179 (2015).
[59] L. S. Mohan, K. K. Rao, and P. R. Nott, A frictional Cosserat model for the slow shearing of granular materials, J. Fluid Mech. **457**, 377 (2002).
[60] N. Mitarai, H. Hayakawa, and H. Nakanishi, Collisional Granular Flow as a Micropolar Fluid, Phys. Rev. Lett. **88**, 174301 (2002).
[61] S. Bharathraj and V. Kumaran, Effect of base topography on flow dynamics and transition in a dense granular flow, J. Fluid Mech. **832**, 600 (2017).
[62] D. L. Henann and K. Kamrin, A predictive, size-dependent continuum model for dense granular flows, Proc. Natl. Acad. Sci. USA **110**, 6730 (2013).
[63] D. Ertas and T. C. Halsey, Granular gravitational collapse and chute flow, Europhys. Lett. **60**, 931 (2002).
[64] O. Baran, D. Ertas, T. C. Halsey, G. S. Grest, and J. B. Lechman, Velocity correlations in dense gravity-driven granular chute flow, Phys. Rev. E **74**, 051302 (2006).
[65] J.-P. Bouchaud, M. E. Cates, J. R. Prakash, and S. F. Edwards, Hysteresis and Metastability in a Continuum Sandpile Model, Phys. Rev. Lett. **74**, 1982 (1995).
[66] S. Torquato, T. M. Truskett, and P. G. Debenedetti, Is Random Close Packing of Spheres Well Defined? Phys. Rev. Lett. **84**, 2064 (2000).
[67] A. J. Liu and S. R. Nagel, Jamming is not just cool any more, Nature (London) **396**, 21 (1998).
[68] I. R. Peters, S. Majumdar, and H. M. Jaeger, Direct observation of dynamic shear jamming in dense suspensions, Nature (London) **532**, 214 (2016).
[69] R. Seto, R. Mari, J. F. Morris, and M. M. Denn, Discontinuous Shear Thickening of Frictional Hard-Sphere Suspensions, Phys. Rev. Lett. **111**, 218301 (2013).
[70] M. Wyart and M. E. Cates, Discontinuous Shear Thickening without Inertia in Dense Non-Brownian Suspensions, Phys. Rev. Lett. **112**, 098302 (2014).
[71] V. Kumaran and S. Maheshwari, Transition due to base roughness in the dense granular flow down an inclined plane, Phys. Fluids **24**, 053302 (2012).
[72] V. Kumaran and S. Bharathraj, The effect of base roughness on the development of a dense granular flow down an inclined plane, Phys. Fluids **25**, 070604 (2013).
[73] S. Mandal and D. V. Khakhar, Sidewall-friction-driven ordering transition in granular channel flows: Implications for granular rheology, Phys. Rev. E **96**, 050901 (2017).
[74] T. Weinhart, A. R. Thornton, S. Luding, and O. Bokhove, Closure relations for shallow granular flows from particle simulations, Granular Matter **14**, 531 (2012).
[75] P. A. Cundall and O. D. L. Strack, A discrete numerical model for granular assemblies, Geotechnique **29**, 47 (1979).